

# Accepted Manuscript

Discovery of unsymmetrical aromatic disulfides as novel inhibitors of SARS-CoV main protease: Chemical synthesis, biological evaluation, molecular docking and 3D-QSAR study

Li Wang, Bo-Bo Bao, Guo-Qing Song, Cheng Chen, Xu-Meng Zhang, Wei Lu, Zefang Wang, Yan Cai, Shuang Li, Sheng Fu, Fu-Hang Song, Haitao Yang, Jian-Guo Wang

PII: S0223-5234(17)30406-3

DOI: [10.1016/j.ejmech.2017.05.045](https://doi.org/10.1016/j.ejmech.2017.05.045)

Reference: EJMECH 9475

To appear in: *European Journal of Medicinal Chemistry*

Received Date: 27 February 2017

Revised Date: 17 May 2017

Accepted Date: 21 May 2017

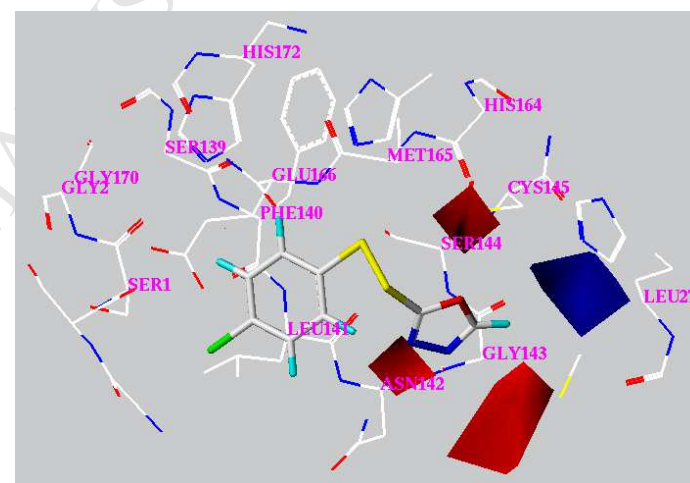
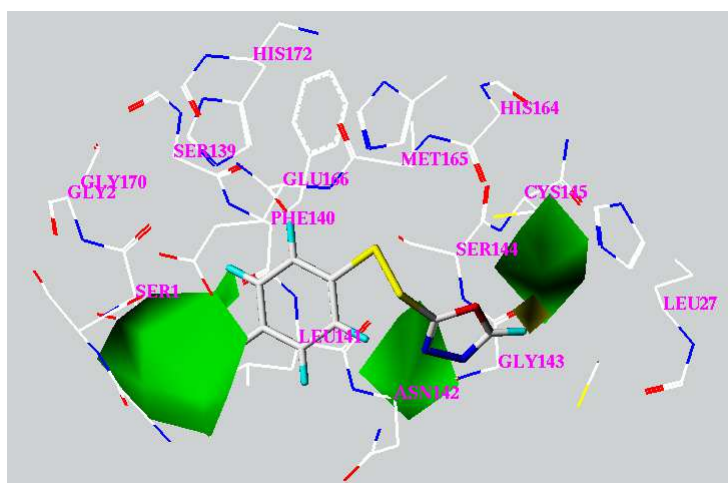
Please cite this article as: L. Wang, B.-B. Bao, G.-Q. Song, C. Chen, X.-M. Zhang, W. Lu, Z. Wang, Y. Cai, S. Li, S. Fu, F.-H. Song, H. Yang, J.-G. Wang, Discovery of unsymmetrical aromatic disulfides as novel inhibitors of SARS-CoV main protease: Chemical synthesis, biological evaluation, molecular docking and 3D-QSAR study, *European Journal of Medicinal Chemistry* (2017), doi: 10.1016/j.ejmech.2017.05.045.

This is a PDF file of an unedited manuscript that has been accepted for publication. As a service to our customers we are providing this early version of the manuscript. The manuscript will undergo copyediting, typesetting, and review of the resulting proof before it is published in its final form. Please note that during the production process errors may be discovered which could affect the content, and all legal disclaimers that apply to the journal pertain.



Discovery of unsymmetrical aromatic disulfides as novel inhibitors of SARS-CoV main protease: Chemical synthesis, biological evaluation, molecular docking and 3D-QSAR study.

Li Wang<sup>a,1</sup>, Bo-Bo Bao<sup>b,c,1</sup>, Guo-Qing Song<sup>a</sup>, Cheng Chen<sup>b,c,\*\*</sup>, Xu-Meng Zhang<sup>a</sup>, Wei Lu<sup>a</sup>, Zefang Wang<sup>b,c</sup>, Yan Cai<sup>b,c</sup>, Shuang Li<sup>b,c</sup>, Sheng Fu<sup>b,c</sup>, Fu-Hang Song<sup>d</sup>, Haitao Yang<sup>b,c</sup>, Jian-Guo Wang<sup>a,\*</sup>



1 Discovery of unsymmetrical aromatic disulfides as novel inhibitors of SARS-CoV main protease:  
2 Chemical synthesis, biological evaluation, molecular docking and 3D-QSAR study.

3

4 Li Wang<sup>a,1</sup>, Bo-Bo Bao<sup>b,c,1</sup>, Guo-Qing Song<sup>a</sup>, Cheng Chen<sup>b,c,\*\*</sup>, Xu-Meng Zhang<sup>a</sup>, Wei Lu<sup>a</sup>, Zefang  
5 Wang<sup>b,c</sup>, Yan Cai<sup>b,c</sup>, Shuang Li<sup>b,c</sup>, Sheng Fu<sup>b,c</sup>, Fu-Hang Song<sup>d</sup>, Haitao Yang<sup>b,c</sup>, Jian-Guo Wang<sup>a,\*</sup>

6

7 *a. State-Key Laboratory and Research Institute of Elemento-Organic Chemistry, National*  
8 *Pesticide Engineering Research Center, College of Chemistry, Nankai University, Tianjin 300071,*  
9 *China*

10 *b. School of Life Sciences, Tianjin University, Tianjin 300072, China.*

11 *c. Tianjin International Joint Academy of Biotechnology and Medicine, Tianjin 300457, China.*

12 *d. CAS Key Laboratory of Pathogenic Microbiology and Immunology, Institute of Microbiology,*  
13 *Chinese Academy of Sciences, Beijing 100101, China*

14

15 <sup>1</sup> These two authors contributed equally to this work.

16

17 \*corresponding author. E-mail address: nkwjg@nankai.edu.cn (J.-G. Wang)

18 \*\* corresponding author. E-mail address: chengchen@tju.edu.cn (C. Chen)

19

20 Abstract: The worldwide outbreak of severe acute respiratory syndrome (SARS) in 2003 had  
21 caused a high rate of mortality. Main protease (M<sup>pro</sup>) of SARS-associated coronavirus  
22 (SARS-CoV) is an important target to discover pharmaceutical compounds for the therapy of this  
23 life-threatening disease. During the course of screening new anti-SARS agents, we have identified  
24 that a series of unsymmetrical aromatic disulfides inhibited SARS-CoV M<sup>pro</sup> significantly for the  
25 first time. Herein, 40 novel unsymmetrical aromatic disulfides were synthesized chemically and  
26 their biological activities were evaluated *in vitro* against SARS-CoV M<sup>pro</sup>. These novel  
27 compounds displayed excellent IC<sub>50</sub> data in the range of 0.516~5.954 μM. Preliminary studies  
28 indicated that these disulfides are reversible and competitive inhibitors. A possible binding mode  
29 was generated via molecular docking simulation and a comparative field analysis (CoMFA) model  
30 was constructed to understand the structure-activity relationships. The present research therefore  
31 has provided some meaningful guidance to design and identify anti-SARS drugs with totally new  
32 chemical structures.

33

34 Keywords: SARS-CoV M<sup>pro</sup>, aromatic disulfide, molecular docking, *in vitro* activity

35

## 36 1. Introduction

37 Severe acute respiratory syndrome (SARS) is a highly infective respiratory disease caused by  
38 SARS coronavirus (SARS-CoV). Its sudden emergence and rapid outbreak during 2002-2003 had

39 resulted in ~800 deaths among >8,000 reported individual cases worldwide [1]. Although the  
40 SARS epidemic had been under control for years, reemergence of this threatening illness is still a  
41 possible risk and potentially new strains of SARS can be more dangerous than the previous ones.  
42 A number of important targets have been recognized to take part in the biological events critical to  
43 SARS-CoV replication, among which a papain-like protease (PL<sup>pro</sup>) and a chymotrypsin-like  
44 protease (3CL<sup>pro</sup>) are of significant importance to design anti-SARS inhibitors [2]. The 3CL<sup>pro</sup>,  
45 also known as the main protease (M<sup>pro</sup>), has attracted much attention, which could be revealed  
46 from numerous publications about novel inhibitor discovery. Crystal structures of SARS-CoV  
47 M<sup>pro</sup>, either free enzyme alone or in complex with an inhibitor, had been determined to facilitate  
48 the structural and functional investigation of this protease [3, 4]. The active site of SARS-CoV  
49 M<sup>pro</sup> contains Cys145 and His41 to constitute a catalytic dyad, in which cysteine functions as the  
50 common nucleophile in the proteolytic process.

51

52 Biological active inhibitors against SARS-CoV M<sup>pro</sup> have been reported mainly from two different  
53 approaches: one is screening large library to identify new active compounds using  
54 high-throughput technique, the other is novel inhibitor design based on the substrate structure or  
55 active site properties rationally [5]. The inhibitory activities of these compounds were then  
56 validated by *in vitro* protease assays. In most cases the kinetic study indicated that the inhibitor is  
57 involved in an irreversible process by forming a covalent bond with Cys145, while in some other  
58 cases the inhibition is actually a reversible behavior. The reported SARS-CoV M<sup>pro</sup> inhibitors  
59 covered a variety of different chemical scaffolds, which contain peptidomimetic compounds,  
60 3-quinoline carboxylic acid derivatives, thiophene-2-carboxylate derivatives, zinc-conjugated  
61 compounds, cinanserin, calmodulin, keto-glutamine analogues, anilide, bifunctional boronic acid  
62 compounds, isatin derivatives, etacrynic acid derivatives, serine derivatives, trifluoromethyl  
63 ketones, acetamides, pyrazolone and quercertins [5-12]. It is a pity that research on drugs and  
64 vaccines towards SARS or SARS-like coronavirus has not brought any candidate for clinical use.  
65 Hence there still exists an urgent need to discover and identify new SARS-CoV M<sup>pro</sup> agents,  
66 especially those compounds from totally new chemical families, to develop effective therapy  
67 against this fatal viral infection.

68

69 Disulfide bonds play essential roles for bioactive proteins to keep correct folding [13]. There are a  
70 few cases that simple disulfides such as diallyl disulfide and dimethyl disulfide exhibit  
71 hypochlorous acid scavenging activity and tyrosinase inhibitory activity (Fig. 1A) [14, 15]. The  
72 unsymmetrical disulfide compounds are useful tools in the research of dynamic combinatorial  
73 chemistry [16]. These compounds have also been reported to display a variety of biological  
74 activities. For examples, Turos et al. reported that some unsymmetrical aryl-alkyl disulfides were  
75 inhibitors of methicillin-resistant *Staphylococcus aureus* and *Bacillus anthracis* (Fig. 1B) [17],  
76 while Khosla and co-workers published some unsymmetrical disulfides that could selectively

77 inhibit extracellular thioredoxin (Fig. 1C) [18]. Yoon et al. showed that some unsymmetrical  
78 disulfide compounds were inhibitors of *Mycobacterium tuberculosis* and *Haemophilus influenzae*,  
79 by interfering with acetohydroxyacid synthase (AHAS), a key enzyme in the biosynthesis pathway  
80 of branched chain amino-acids (Fig. 1D) [19, 20]. In the past of our research, we found that some  
81 unsymmetrical aromatic disulfides could inhibit plant AHAS and was useful for herbicide research  
82 (Fig. 1E) [21, 22].

83

84 There are indeed a few reports that some aromatic disulfides exhibit antiviral activity. The  
85 virucidal activity of NSC4492 was due to targeting of arenavirus RNA synthesis (Fig. 1F) [23],  
86 while 5,5'-dithiobis-2-nitrobenzoic acid (DTNB) had antiviral properties against T-tropic human  
87 immunodeficiency virus type 1 (HIV-1) (Fig. 1G) [24]. An antiviral disulfide NSC20625  
88 compound could block interaction between arenavirus Z protein and cellular promyelocytic  
89 leukemia protein (Fig. 1H) [25]. However, the antiviral activities against arenavirus might be  
90 different from that against coronavirus. There is no evidence that the reported antiviral activities  
91 of aromatic disulfides have any direct relationships with SARS-CoV M<sup>pro</sup> inhibition.

92

93 In an effort to discover novel inhibitors of SARS-CoV M<sup>pro</sup>, we have synthesized a series of novel  
94 unsymmetrical aromatic disulfides and evaluated their biological activities in this study. The target  
95 compounds could inhibit main protease of SARS-CoV remarkably, with the best  $IC_{50}$  value of  
96 0.516  $\mu$ M. Subsequent enzymatic kinetics study indicated that the aromatic disulfides acted as  
97 reversible and non-competitive inhibitors. Therefore we have demonstrated that unsymmetrical  
98 disulfide compounds with aromatic rings are novel inhibitors of SARS-CoV M<sup>pro</sup> from a totally  
99 new chemical family, which will provide helpful information for further drug discovery.

100

## 101 2. Results and discussion

102

### 103 2.1. Chemistry of the target compounds

104 The target unsymmetrical disulfides were synthesized by the reaction of various substituted  
105 2-mercapto-[1,3,4]oxadiazole, substituted 2-mercapto-thiazole, substituted 2-mercapto-  
106 1*H*-imidazole or substituted 2-mercapto-pyrimidine with substituted arenesulfonyl chloride in  
107 ethyl ether under very mild condition as reported previously [21, 22]. It is a quite straightforward  
108 nucleophilic substitution, in which the thiol group in the mercapto compound serves as a  
109 nucleophilic reagent and attacks the sulfur atom in the arenesulfonyl chloride. Most yields for the  
110 reactions were satisfactory, showing that this is a simple and easy procedure to produce  
111 unsymmetrical aromatic disulfides, superior to the synthetic route developed by Hahn et al [26]. In  
112 Hahn's paper, moist tetrahydrofuran gave better yields than dried benzene as the solvent for the  
113 reaction, so the authors added 5–10 M equivalent of water to the reaction mixture and observed  
114 satisfactory yields. Thus, the presence of water was thought to be preferable for the reaction by

115 Hahn et al [26]. In our synthesis experiment, only ethyl ether was used as the solvent and no  
116 additional water was added to the reaction, nevertheless, we observed very high yields for most of  
117 the target compounds.

118

119 The -S-S- bond had been confirmed in our previous paper [21]. Compound **3-4**, **3-6**, **3-7**, **3-8**, **3-9**,  
120 **3-10** and **3-11** were further acetylated from corresponding parent compounds that had been  
121 published by us [21]. The molecular structures of the compounds are listed in Table 1. The title  
122 compounds were fully characterized by  $^1\text{H}$  NMR,  $^{13}\text{C}$  NMR and HRMS (Part 1 of the  
123 supplementary data for the original figures).

124

## 125 2.2. *In vitro* inhibitory activity of SARS-CoV M<sup>pro</sup>

126 All the synthesized unsymmetrical aromatic disulfides were subjected to the *in vitro* assay of  
127 SARS-CoV M<sup>pro</sup>. The results are also illustrated in Table 1, expressed by  $IC_{50}$  values. It could be  
128 seen that the target compounds exhibited encouraging biological potency, with excellent  $IC_{50}$   
129 values ranging from 0.516  $\mu\text{M}$  to 5.954  $\mu\text{M}$  (The inhibition curves of all target compounds can be  
130 found in part 2 of the supplementary data). This was surprising due to the fact that not any  
131 research group had ever identified the disulfide compounds as inhibitors of SARS-CoV M<sup>pro</sup>, not  
132 to mention such strong inhibition.

133

134 Inhibition type of the disulfides was determined by means of enzymatic kinetic study, for which  
135 **3-31** and **3-39** were used. From Fig. 2 it can be seen that in the plot of enzyme concentration  
136 versus reaction velocity, the lines represent different inhibitor concentrations intersect at a same  
137 point, suggesting that the inhibition is actually a reversible action. We then measured the  
138 enzymatic velocity of SARS-CoV M<sup>pro</sup> versus substrate concentrations in the presence of either  
139 **3-31** or **3-39** (Part 3 of the supplementary data). The lines displayed in reciprocal plots intersect at  
140 a same point, indicating that both inhibitors serve as a non-competitive inhibitor with  $\alpha < 1$  (Part 3  
141 of the supplementary data) [27]. On this basis, the kinetic parameters ( $\alpha K_i = 0.20 \mu\text{M}$ ,  $K_i = 0.24$   
142  $\mu\text{M}$ ) of **3-31** were determined [28] (Fig. 3), which clearly proved that, the non-competitive  
143 inhibitor **3-31** is characterized by smaller equilibrium-binding constant compared to some known  
144 inhibitors such as N3 ( $K_i = 9.0 \mu\text{M}$ ) and N9 ( $K_i = 6.7 \mu\text{M}$ ) [3].

145

146 Since there is a cysteine in the active site of SARS-CoV M<sup>pro</sup> (Cys145), which plays an essential  
147 role for the biological activity of this protease, it is possible that the disulfide compound reacts  
148 with Cys145 to form a new -S-S- bond and results in a loss of enzyme activity. It is known that, if  
149 a disulfide reacts with another thiol to give a new disulfide, the thiols that are parts of the old  
150 disulfide can also react directly with this thiol to form the same new disulfide [29]. We tested the  
151 biological activities of different aryl thiols derived from our disulfides, and no inhibition of  
152 SARS-CoV M<sup>pro</sup> could be detected for any of them even at very high concentration. Accordingly it

153 seemed unlikely that Cys145 formed a -S-S- bond by reacting with the target disulfide compounds.  
154 Another method to rule out this possibility is to determine the change of the molecular weight of  
155 the protein before and after inhibition [30, 31]. If the disulfide compound reacts with Cys145, the  
156 molecular weight would have a shift after SARS-CoV M<sup>pro</sup> is inhibited, and this is approximately  
157 the mass of half moiety of the unsymmetrical disulfide. Bearing this in mind, we measured the  
158 molecular weight of protease before and after inhibition by three disulfide compounds with  
159 significant structure difference (**3-8**, **3-31** and **3-39**, data shown in part 4 of the supplementary  
160 data). However, no such assumed shift in the molecular weight was observed to support this idea.

161

162 For another possibility, Khosla et al. had reported selective inhibition of extracellular thioredoxin  
163 by unsymmetrical disulfides [18], in which two cysteine residues in a close distance form an  
164 intramolecular disulfide bond. After careful analysis of the SARS-CoV M<sup>pro</sup> crystal structure (pdb  
165 entry 2AMD) [3], no other cysteine residue was found to be in a nearby space of Cys145. In fact  
166 not any two cysteine residues are in a reasonable distance to form possible intramolecular  
167 disulfide bond. Thus we also denied this probable inhibitory mechanism.

168

### 169 2.3. Molecular docking and three dimensional structure-activity relationships

170 Since the unsymmetrical aromatic disulfides do not react with the residues of the SARS-CoV M<sup>pro</sup>,  
171 it means that these compounds act as intact molecules when inhibiting this protease. Therefore, in  
172 silico molecular docking technique was utilized to predict possible binding modes of the disulfide  
173 compounds with SARS-CoV M<sup>pro</sup>. In our previous study, we had docked a small library of isatin  
174 compounds to the active site of AHAS and probable binding modes were predicted by FlexX  
175 [32-37]. Here similar strategy was adopted to carry out database docking. After investigation of  
176 the resulting docked conformations, nineteen compounds were found to overlay one another quite  
177 well (Part 5 of the supplementary data), while all the other twenty-one compounds were in  
178 unreasonable binding space, and they failed to overlay well with one another. Thus, the docked  
179 conformations of the nineteen compounds were thought to be the possible binding conformations  
180 in this study. Compound **3-31** was chosen to depict the binding mode of the disulfide inhibitors.  
181 Fig. 4 is a two-dimensional illustration of the interactions between the inhibitor and the  
182 surrounding residues of SARS-CoV M<sup>pro</sup> drawn by LIGPLOT [38]. The location of **3-31** has some  
183 overlap with the inhibitor N9, the inhibitor in the original pdb file. The compound binds with  
184 SARS-CoV M<sup>pro</sup> via multiple hydrogen bonding contacts and hydrophobic contacts. Phe140,  
185 Leu141, His163, Met165, Glu166 and His172 form hydrophobic interactions with the small  
186 molecule, while Asn142, Gly143 and Cys145 form intermolecular H-bond with the inhibitor. The  
187 predicted binding mode therefore provides a useful clue to understand the possible molecular basis  
188 of these inhibitors.

189

190 Comparative field analysis (CoMFA) is a tool to generate 3D contour models to quantitatively

191 analyze the structure-activity relationships of bioactive compounds by steric and electrostatic  
192 contributions [39-41]. On the basis of the docked conformation, the molecules in the database  
193 were aligned to construct a CoMFA model. Compounds **3-8**, **3-23** and **3-40** were excluded from  
194 the database because they were statistical outliers in the training set, that is, the inclusion of any of  
195 these molecules did not yield a satisfactory leave-one-out  $q^2$ . The training set without the outliers  
196 gave a leave-one-out  $q^2$  of 0.681 when the optimum components was 6, and the  
197 non-crossvalidated  $r^2$  was 0.916, with a standard error of estimate of 0.088 and F values of 37.968.  
198 The steric and electrostatic contributions were 43.6% and 56.4%, respectively.

199

200 Compound **3-31** was used to illustrate the steric and electrostatic contour maps, together with the  
201 neighboring residues in the docked binding pocket (Fig. 5). For the steric contour map, a bulky  
202 group is favorable for better inhibition in the green contour region and such a group is likely to  
203 decrease the activity in the yellow contour space. The green maps are mostly in three bulks: one  
204 formed by Ser141 and Leu141, one formed by Asn142 and Gly143 and the last one formed by  
205 Ser144 and Cys145; whereas the yellow maps are just located in a space nearby Gly143. For the  
206 electrostatic contour map, in the blue contour region, an increase in the positive charge will lead to  
207 an increase of activity, yet in the red contour region, negative charge is favorable to enhance the  
208 activity. The blue map is in a region surrounded by Leu27, Cys143, Ser144 and Cys145, whereas  
209 the red maps are in three cavities: one formed by Leu141 and Asn142, one formed by Ser144,  
210 Cys145 and Met165 and the last one formed by Asn142 and Gly143. The 3D CoMFA maps have  
211 afforded important structural features of the unsymmetrical aromatic disulfides from steric and  
212 electrostatic views, which is valuable for further design and discovery of more potent inhibitors.

213

### 214 **3. Conclusion**

215 The lack of effective anti-SARS agents makes it a possible danger when SARS breaks out  
216 sometime in the future, numerous people will be killed again. Therefore it is still an urgent  
217 demand to discover novel anti-SARS inhibitors to combat this deadly disease. SARS CoV M<sup>pro</sup> is  
218 an important target for the design of therapeutically useful drugs. In the present study, in an effort  
219 to develop non-peptidic anti-SARS inhibitors, we have identified for the first time, that some  
220 unsymmetrical aromatic disulfides are excellent inhibitors of SARS CoV M<sup>pro</sup>, the mechanism of  
221 which seems distinct as they are reversible and competitive inhibitors. This suggests that the  
222 unsymmetrical disulfides are promising lead compounds identification and development of a new  
223 family of biologically active anti-SARS agents. A possible binding model of the disulfide inhibitor  
224 was built by molecular docking, and a CoMFA model was constructed subsequently to point out  
225 the structural features of these novel inhibitors of SARS CoV M<sup>pro</sup>. Based on this information,  
226 further structural modifications are ongoing for better pharmaceutical compounds. The Lipinski  
227 rules will also be utilized to help to develop compounds with a final *in vivo* activity [42]. We are  
228 also trying to co-crystallize the protease and the best inhibitor, to gain insight into a real binding

229 mode and explain the molecular basis of these compounds.

230

## 231 4. Experimental section

232

### 233 4.1. General synthesis and instruments

234 Various heterocyclic aromatic thiols **1** were commercial procured from 5A Pharmatech (China),  
235 Apichemical (China), Aldrich and ACES pharma, which were all >95% purity grade. All solvents  
236 and liquid reagents were dried in advance using standard methods and distilled before use.  
237 Substituted arenesulfenyl chlorides **2** were synthesized as described in our previous publications  
238 [21, 22]. Synthetic methods for compounds **3'** had been reported and these parent compounds for  
239 **3-4, 3-6, 3-7, 3-8, 3-9, 3-10** and **3-11** had also been fully characterized before [21]. Melting points  
240 were determined using an X-4 melting apparatus and were uncorrected. <sup>1</sup>H NMR spectra and <sup>13</sup>C  
241 NMR were obtained using a 400 MHz Varian Mercury Plus 400 spectrometer. The chemical shift  
242 values (δ) for the NMR spectra were reported as parts per million (ppm), using deuterated  
243 chloroform (CDCl<sub>3</sub>) or dimethyl sulfoxide (DMSO-*d*<sub>6</sub>) as the solvent and tetramethylsilane (TMS)  
244 as an internal reference standard. Mass spectra were recorded on a Thermo Finnigan LCQ  
245 Advantage LC/mass detector instrument.

246

### 247 4.2. Synthesis of the target compounds (Scheme 1.)

248 Heterocyclic aromatic thiols (**1**, 5mmol) was added to a solution of freshly prepared arenesulfenyl  
249 chlorides (**2**, 5 mmol) in 25 mL of anhydrous ethyl ether at room temperature. The mixture was  
250 then stirred for 5 h at the same temperature, after that the solvent was removed under reduced  
251 pressure. Products **3** (**3'** for **3-4, 3-6, 3-7, 3-8, 3-9, 3-10** and **3-11**) were purified by column  
252 chromatography in 75-95% yields.

253

### 254 4.3. Synthesis of the compounds **3-4, 3-6, 3-7, 3-8, 3-9, 3-10** and **3-11** (Scheme 2.)

255 Unsymmetrical aromatic disulfide (**3'**, 5mmol) was added to 10 mL of acetic anhydride. The  
256 reaction mixture was stirred for 0.5h at 60 °C and then 200 mL water was added to the mixture.  
257 The pH value was adjusted by sodium bicarbonate to 7~8. The product was extracted by ethyl  
258 acetate and the solvent was removed under reduced pressure. The target compounds were finally  
259 purified by column chromatography in 87-95% yields.

260

### 261 4.4. Characterization of the target compounds

#### 262 4.4.1. 2-((4-chlorophenyl)disulfanyl)thiazole (**3-1**)

263 Yield 89%; m.p.: 114-116 °C; yellow solid; <sup>1</sup>H NMR (400 MHz, DMSO-*d*<sub>6</sub>), δ 7.62 (d, *J* = 8.5 Hz,  
264 2H, ArH), 7.47 (d, *J* = 8.5 Hz, 2H, ArH), 7.31 (s, 1H, NCH), 6.99 (d, *J* = 4.3 Hz, 1H, SCH); <sup>13</sup>C  
265 NMR (101 MHz, DMSO-*d*<sub>6</sub>), δ 134.8, 132.2, 129.3, 121.9, 114.20, 99.7; HRMS(MALDI) *m/z*:  
266 calculated for C<sub>9</sub>H<sub>6</sub>ClNS<sub>3</sub> 259.9423, found 259.9420 [M + H]<sup>+</sup>.

267

268 4.4.2. *N*-(2-(*p*-tolylidisulfanyl)thiazol-5-yl)acetamide (3-2)

269 Yield 91%; m.p.: 113-115 °C; yellow solid; <sup>1</sup>H NMR (400 MHz, DMSO-*d*<sub>6</sub>), δ 11.70 (s, 1H, NH),  
270 7.50 (d, *J* = 6.5 Hz, 2H, ArH), 7.47 (s, 1H, CH), 7.26 (d, *J* = 7.8 Hz, 2H, ArH), 2.32 (s, 3H, CH<sub>3</sub>),  
271 2.10 (s, 3H, CH<sub>3</sub>); <sup>13</sup>C NMR (101 MHz, DMSO-*d*<sub>6</sub>), 167.6, 154.1, 138.9, 132.3, 130.6, 130.0,  
272 128.4, 22.6, 21.1; HRMS(MALDI) *m/z*: calculated for C<sub>12</sub>H<sub>12</sub>N<sub>2</sub>OS<sub>3</sub> 297.0185, found 297.0185  
273 [M + H]<sup>+</sup>.

274

275 4.4.3. ethyl 2-((4-chlorophenyl)disulfanyl)-1*H*-imidazole-4-carboxylate (3-3)

276 Yield 87%; m.p.: 100-102 °C; yellow solid; <sup>1</sup>H NMR (400 MHz, DMSO-*d*<sub>6</sub>), δ 7.98 (s, 1H), 7.64  
277 (d, *J* = 8.6 Hz, 2H, ArH), 7.49 (d, *J* = 8.6 Hz, 2H, ArH), 4.24 (q, *J* = 7.0 Hz, 2H, CH<sub>2</sub>CH<sub>3</sub>), 1.27 (t,  
278 *J* = 7.1 Hz, 3H, CH<sub>2</sub>CH<sub>3</sub>); <sup>13</sup>C NMR (101 MHz, DMSO-*d*<sub>6</sub>), δ 161.1, 132.9, 131.7, 128.7, 117.1,  
279 116.9, 60.5, 14.7; HRMS(MALDI) *m/z*: calculated for C<sub>12</sub>H<sub>11</sub>ClN<sub>2</sub>O<sub>2</sub>S<sub>2</sub> 315.0022, found 315.0021  
280 [M + H]<sup>+</sup>.

281

282 4.4.4. 1-(5-methyl-3-((2-nitrophenyl)disulfanyl)-1*H*-1,2,4-triazol-1-yl)ethanone (3-4)

283 Yield 90%; m.p.: 157-159 °C; yellow solid; <sup>1</sup>H NMR (400 MHz, DMSO-*d*<sub>6</sub>), δ 8.31 (d, *J* = 8.2 Hz,  
284 1H), 8.24 (d, *J* = 8.2 Hz, 1H), 7.91 (t, *J* = 7.7 Hz, 1H), 7.58 (t, *J* = 7.8 Hz, 1H), 2.59 (s, 3H), 2.55  
285 (s, 3H); <sup>13</sup>C NMR (101 MHz, DMSO-*d*<sub>6</sub>), δ 169.3, 157.8, 157.3, 144.9, 135.6, 134.3, 127.9, 126.6,  
286 23.5, 15.6; HRMS(MALDI) *m/z*: calculated for C<sub>11</sub>H<sub>10</sub>N<sub>4</sub>O<sub>3</sub>S<sub>2</sub> 311.0273, found 311.0261 [M + H]  
287 <sup>+</sup>.

288

289 4.4.5. *N*-(2-(phenyl)disulfanyl)thiazol-5-yl)acetamide (3-5)

290 Yield 89%; m.p.: 108-110 °C; yellow solid; <sup>1</sup>H NMR (400 MHz, DMSO-*d*<sub>6</sub>), δ 11.79 (s, 1H, NH),  
291 7.64 (t, *J* = 8.6 Hz, 2H, ArH), 7.53 (d, *J* = 8.5 Hz, 1H, ArH), 7.51 – 7.42 (m, 2H, ArH), 7.39 (d, *J*  
292 = 7.1 Hz, 1H, ArH), 2.10 (s, 3H, CH<sub>3</sub>); <sup>13</sup>C NMR (101 MHz, DMSO-*d*<sub>6</sub>), δ 167.6, 139.4, 137.2,  
293 130.8, 130.0, 129.9, 129.0, 128.8, 128.42, 22.6; HRMS(MALDI) *m/z*: calculated for C<sub>11</sub>H<sub>10</sub>N<sub>2</sub>OS<sub>3</sub>  
294 283.0029, found 283.0031 [M + H]<sup>+</sup>.

295

296 4.4.6. 1-(5-phenyl-3-(*p*-tolylidisulfanyl)-1*H*-1,2,4-triazol-1-yl)ethanone (3-6)

297 Yield 92%; m.p.: 112-114 °C; white solid; <sup>1</sup>H NMR (400 MHz, DMSO-*d*<sub>6</sub>), δ 8.35 (d, *J* = 17.6 Hz,  
298 1H), 8.00 (d, *J* = 8.1 Hz, 2H), 7.79 (d, *J* = 7.6 Hz, 3H), 7.56 (t, *J* = 7.6 Hz, 1H), 7.27 (s, 2H), 2.72  
299 (s, 3H), 2.33 (s, 3H); <sup>13</sup>C NMR (101 MHz, DMSO-*d*<sub>6</sub>), δ 135.4, 129.4, 128.9, 128.1, 126.2, 125.8,  
300 129.5, 22.2, 20.8; HRMS(MALDI) *m/z*: calculated for C<sub>17</sub>H<sub>15</sub>N<sub>3</sub>OS<sub>2</sub> 342.0729, found 342.0734  
301 [M + H]<sup>+</sup>.

302

303 4.4.7. 1-(3-((4-methoxyphenyl)disulfanyl)-5-phenyl-1*H*-1,2,4-triazol-1-yl)ethanone (3-7)

304 Yield 91%; m.p.: 133-135 °C; white solid; <sup>1</sup>H NMR (400 MHz, DMSO-*d*<sub>6</sub>), δ 8.11 (s, 2H), 7.70 (d,

305  $J = 7.3$  Hz, 2H), 7.38 (s, 3), 6.73 (d,  $J = 7.2$  Hz, 2H), 3.65 (s, 3H), 2.58 (s, 3H);  $^{13}\text{C}$  NMR (101  
306 MHz, DMSO- $d_6$ ),  $\delta$  169.3, 161.9, 161.2, 158.9, 134.8, 129.9, 129.3, 128.5, 127.1, 124.8, 115.0,  
307 55.2, 22.5; HRMS(MALDI)  $m/z$ : calculated for  $\text{C}_{17}\text{H}_{15}\text{N}_3\text{O}_2\text{S}_2$  358.0683, found 358.0685  $[\text{M}+\text{H}]^+$ .

308

309 **4.4.8. 1-(3-((2-nitrophenyl)disulfanyl)-5-(pyridin-3-yl)-1H-1,2,4-triazol-1-yl)ethanone (3-8)**

310 Yield 89%; m.p.: 186-188  $\square$ ; yellow solid;  $^1\text{H}$  NMR (400 MHz,  $\text{CDCl}_3$ ),  $\delta$  8.64 (d,  $J = 4.6$  Hz,  
311 1H), 7.95 (d,  $J = 4.8$  Hz, 1H), 7.70 – 7.42 (m, 1H), 7.33 (d,  $J = 8.4$  Hz, 2H), 7.21 (d,  $J = 8.7$  Hz,  
312 3H), 3.06 (s, 3H);  $^{13}\text{C}$  NMR (101 MHz,  $\text{CDCl}_3$ ),  $\delta$  174.9, 150.1, 135.3, 129.9, 129.5, 129.3, 127.5,  
313 120.7, 46.0, 29.7; HRMS(MALDI)  $m/z$ : calculated for  $\text{C}_{15}\text{H}_{11}\text{N}_5\text{O}_3\text{S}_2$  374.0381, found 374.0380  
314  $[\text{M}+\text{H}]^+$ .

315

316 **4.4.9. ethyl 2-((1-acetyl-5-(pyridin-3-yl)-1H-1,2,4-triazol-3-yl)disulfanyl)benzoate (3-9)**

317 Yield 92%; m.p.: 128-130  $\square$ ; white solid;  $^1\text{H}$  NMR (400 MHz, DMSO- $d_6$ ),  $\delta$  9.10 (s, 1H), 8.66 (s,  
318 1H), 8.26 (d,  $J = 7.8$  Hz, 2H), 8.00 (d,  $J = 7.5$  Hz, 1H), 7.75 (s, 1H), 7.57 (d,  $J = 7.2$  Hz, 1H), 7.41  
319 (s, 1H), 4.22 (q, 2H), 2.50 (s, 3H), 1.33 (t,  $J = 7.1$  Hz, 3H);  $^{13}\text{C}$  NMR (101 MHz, DMSO- $d_6$ ),  $\delta$   
320 150.1, 135.1, 133.6, 130.9, 129.5, 129.3, 120.7, 45.9, 29.7, 22.5, 8.7; HRMS(MALDI)  $m/z$ :  
321 calculated for  $\text{C}_{18}\text{H}_{16}\text{N}_4\text{O}_3\text{S}_2$  401.0736, found 401.0746  $[\text{M} + \text{H}]^+$ .

322

323 **4.4.10. ethyl 2-((1-acetyl-5-(pyridin-4-yl)-1H-1,2,4-triazol-3-yl)disulfanyl)benzoate (3-10)**

324 Yield 95%; m.p.: 130-132  $\square$ ; white solid;  $^1\text{H}$  NMR (400 MHz, DMSO- $d_6$ ),  $\delta$  9.10 (s, 1H), 8.66  
325 (s, 1H), 8.26 (d,  $J = 7.8$  Hz, 2H), 8.00 (d,  $J = 7.5$  Hz, 1H), 7.75 (t,  $J = 7.6$  Hz, 1H), 7.54 (s, 1H), 7.41  
326 (t,  $J = 7.2$  Hz, 1H), 4.34 (q,  $J = 7.1$  Hz, 2H), 2.50 (s, 3H), 1.33 (t,  $J = 7.1$  Hz, 3H);  $^{13}\text{C}$  NMR (101  
327 MHz, DMSO- $d_6$ ),  $\delta$  167.9, 150.1, 135.1, 133.6, 130.9, 129.5, 129.3, 120.7, 45.9, 29.7, 8.6;  
328 HRMS(MALDI)  $m/z$ : calculated for  $\text{C}_{18}\text{H}_{16}\text{N}_4\text{O}_3\text{S}_2$  401.0737, found 401.0746  $[\text{M} + \text{H}]^+$ .

329

330 **4.4.11. 1-(3-((4-methoxyphenyl)disulfanyl)-5-(pyridin-3-yl)-1H-1,2,4-triazol-1-yl)ethanone (3-11)**

331 Yield 87%; m.p.: 113-115  $\square$ ; white solid;  $^1\text{H}$  NMR (400 MHz, DMSO- $d_6$ ),  $\delta$  9.32 (d,  $J = 37.6$  Hz,  
332 1H), 8.53 (d,  $J = 5.9$  Hz, 2H), 7.72 (d,  $J = 8.5$  Hz, 1H), 7.54 – 7.27 (m, 2H), 6.76 (d,  $J = 8.8$  Hz,  
333 2H), 3.70 (s, 3H), 2.64 (s, 3H);  $^{13}\text{C}$  NMR (101 MHz, DMSO- $d_6$ ),  $\delta$  161.0, 160.3, 150.9, 148.3,  
334 135.8, 134.0, 123.7, 115.0, 114.7, 55.4, 29.7; HRMS(MALDI)  $m/z$ : calculated for  $\text{C}_{16}\text{H}_{14}\text{N}_4\text{O}_2\text{S}_2$   
335 359.0630, found 359.0639  $[\text{M} + \text{H}]^+$ .

336

337 **4.4.12. N-(2-((4-chlorophenyl)disulfanyl)thiazol-5-yl)acetamide (3-12)**

338 Yield 94%; m.p.: 127-129  $\square$ ; yellow solid;  $^1\text{H}$  NMR (400 MHz, DMSO- $d_6$ ),  $\delta$  11.73 (s, 1H, NH),  
339 7.65 (d,  $J = 8.6$  Hz, 2H, ArH), 7.52 (d,  $J = 8.5$  Hz, 2H, ArH), 7.48 (s, 1H, CH), 2.10 (s, 3H,  $\text{CH}_3$ );  
340  $^{13}\text{C}$  NMR (101 MHz, DMSO- $d_6$ ),  $\delta$  167.6, 153.1, 152.0, 139.3, 134.4, 133.6, 130.8, 129.9, 128.5,  
341 22.6; HRMS(MALDI)  $m/z$ : calculated for  $\text{C}_{11}\text{H}_9\text{ClN}_2\text{OS}_3$  316.9639, found 316.9641  $[\text{M} + \text{H}]^+$ .

342

343 4.4.13. *N*-(2-((4-bromophenyl)disulfanyl)thiazol-5-yl)acetamide (**3-13**)

344 Yield 93%; m.p.: 123-125 °C; yellow solid; <sup>1</sup>H NMR (400 MHz, DMSO-*d*<sub>6</sub>), δ 11.72 (s, 1H, NH),  
 345 7.65 (d, *J* = 8.6 Hz, 2H, ArH), 7.58 (d, *J* = 8.6 Hz, 2H, ArH), 7.48 (s, 1H, CH), 2.10 (s, 3H, CH<sub>3</sub>);  
 346 <sup>13</sup>C NMR (101 MHz, DMSO-*d*<sub>6</sub>), δ 167.5, 167.0, 152.0, 139.6, 132.4, 130.5, 128.0, 121.6, 22.2;  
 347 HRMS(MALDI) *m/z*: calculated for C<sub>11</sub>H<sub>9</sub>BrN<sub>2</sub>O<sub>3</sub> 360.9132, found 360.9128 [M + H]<sup>+</sup>.

348

349 4.4.14. methyl 2-((2-nitrophenyl)disulfanyl)-1*H*-imidazole-4-carboxylate (**3-14**)

350 Yield 88%; m.p.: 160-163 °C; yellow solid; <sup>1</sup>H NMR (400 MHz, DMSO-*d*<sub>6</sub>), δ 8.51 (d, *J* = 8.2 Hz,  
 351 1H, ArH), 8.31 (dd, *J* = 8.2, 1.1 Hz, 1H, ArH), 7.98 (s, 1H), 7.96 (s, 1H, NHCH), 7.58 (dd, *J* =  
 352 11.4, 4.1 Hz, 1H, ArH), 3.74 (s, 3H, OCH<sub>3</sub>); <sup>13</sup>C NMR (101 MHz, DMSO-*d*<sub>6</sub>), δ 158.9, 151.1,  
 353 139.8, 137.7, 131.2, 130.5, 129.4, 125.2, 124.4, 122.2, 53.0; HRMS(MALDI) *m/z*: calculated for  
 354 C<sub>11</sub>H<sub>9</sub>N<sub>3</sub>O<sub>4</sub>S<sub>2</sub> 312.0107, found 312.0112 [M + H]<sup>+</sup>.

355

356 4.4.15. methyl 2-((2-(ethoxycarbonyl)phenyl)disulfanyl)-1*H*-imidazole-4-carboxylate (**3-15**)

357 Yield 92%; m.p.: 93-95 °C; yellow solid; <sup>1</sup>H NMR (400 MHz, DMSO-*d*<sub>6</sub>), δ 8.34 (d, *J* = 8.2 Hz,  
 358 1H, ArH), 8.03 – 7.96 (m, 1H, ArH), 7.96 (s, 1H, NHCH), 7.79 – 7.66 (m, 1H, ArH), 7.41 (t, *J* =  
 359 7.5 Hz, 1H, ArH), 4.32 (q, *J* = 7.1 Hz, 2H, CH<sub>2</sub>CH<sub>3</sub>), 3.74 (s, 3H, OCH<sub>3</sub>), 1.32 (t, *J* = 7.1 Hz, 3H,  
 360 CH<sub>2</sub>CH<sub>3</sub>); <sup>13</sup>C NMR (101 MHz, DMSO-*d*<sub>6</sub>), δ 166.1, 161.8, 157.8, 141.0, 139.9, 134.1, 131.5,  
 361 126.9, 126.8, 126.5, 121.9, 61.9, 51.8, 14.5; HRMS(MALDI) *m/z*: calculated for C<sub>14</sub>H<sub>14</sub>N<sub>2</sub>O<sub>4</sub>S<sub>2</sub>  
 362 339.0468, found 339.0475 [M + H]<sup>+</sup>.

363

364 4.4.16. methyl 2-((2-(methoxycarbonyl)phenyl)disulfanyl)-1*H*-imidazole-4-carboxylate (**3-16**)

365 Yield 89%; m.p.: 114-116 °C; yellow solid; <sup>1</sup>H NMR (400 MHz, DMSO-*d*<sub>6</sub>), δ 8.35 (d, *J* = 8.2 Hz,  
 366 1H, ArH), 8.00 (d, *J* = 7.8 Hz, 1H, ArH), 7.95 (s, 1H, NHCH), 7.76 (t, *J* = 7.8 Hz, 1H, ArH), 7.41  
 367 (t, *J* = 7.5 Hz, 1H, ArH), 3.87 (s, 3H, OCH<sub>3</sub>), 3.74 (s, 3H, OCH<sub>3</sub>); <sup>13</sup>C NMR (101 MHz,  
 368 DMSO-*d*<sub>6</sub>), δ 158.9, 137.8, 134.2, 131.9, 129.6, 128.9, 127.8, 126.9, 125.2, 124.4, 53.2, 52.4;  
 369 HRMS(MALDI) *m/z*: calculated for C<sub>13</sub>H<sub>12</sub>N<sub>2</sub>O<sub>4</sub>S<sub>2</sub> 325.0311, found 325.0314 [M + H]<sup>+</sup>.

370

371 4.4.17. methyl 2-((4-chlorophenyl)disulfanyl)-1*H*-imidazole-4-carboxylate (**3-17**)

372 Yield 89%; m.p.: 138-140 °C; yellow solid; <sup>1</sup>H NMR (400 MHz, DMSO-*d*<sub>6</sub>), δ 8.00 (s, 1H,  
 373 NHCH), 7.64 (d, *J* = 8.6 Hz, 2H, ArH), 7.49 (d, *J* = 8.7 Hz, 2H, ArH), 3.76 (s, 3H, OCH<sub>3</sub>); <sup>13</sup>C  
 374 NMR (101 MHz, DMSO-*d*<sub>6</sub>), δ 158.7, 147.5, 137.8, 133.5, 129.9, 128.2, 127.9, 125.2, 124.4, 53.2;  
 375 HRMS(MALDI) *m/z*: calculated for C<sub>11</sub>H<sub>9</sub>ClN<sub>2</sub>O<sub>2</sub>S<sub>2</sub> 300.9867, found 300.9894 [M + H]<sup>+</sup>.

376

377 4.4.18. *N*-(2-((4-fluorophenyl)disulfanyl)thiazol-5-yl)acetamide (**3-18**)

378 Yield 95%; m.p.: 119-122 °C; yellow solid; <sup>1</sup>H NMR (400 MHz, DMSO-*d*<sub>6</sub>), δ 11.78 (s, 1H, NH),  
 379 7.68 (d, *J* = 8.6 Hz, 2H, ArH), 7.50 (s, 1H, CH), 7.32 (t, *J* = 8.3 Hz, 2H, ArH), 2.11 (s, 3H, CH<sub>3</sub>);  
 380 <sup>13</sup>C NMR (101 MHz, DMSO-*d*<sub>6</sub>), δ 167.4, 153.8, 139.4, 132.6, 132.5, 131.5, 128.5, 117.3, 117.1,

381 22.6; HRMS(MALDI) m/z: calculated for C<sub>11</sub>H<sub>9</sub>FN<sub>2</sub>OS<sub>3</sub> 300.9934, found 300.9934 [M + H]<sup>+</sup>.

382

383 4.4.19. *N*-(2-((2-nitrophenyl)disulfanyl)thiazol-5-yl)acetamide (**3-19**)

384 Yield 93%; m.p.: 130-133 °C; yellow solid; <sup>1</sup>H NMR (400 MHz, DMSO-*d*<sub>6</sub>), δ 11.76 (s, 1H, NH),  
385 8.41 (d, *J* = 7.9 Hz, 1H, ArH), 8.35 (d, *J* = 8.5 Hz, 1H, ArH), 7.96 (d, *J* = 7.4 Hz, 1H, ArH), 7.61 (t,  
386 *J* = 7.4 Hz, 1H, ArH), 7.49 (s, 1H CH), 2.09 (s, 3H, CH<sub>3</sub>); <sup>13</sup>C NMR (101 MHz, DMSO-*d*<sub>6</sub>), δ  
387 167.6, 151.4, 145.3, 139.4, 135.8, 134.8, 128.4, 128.3, 127.8, 126.8, 22.5; HRMS(MALDI) m/z:  
388 calculated for C<sub>11</sub>H<sub>9</sub>N<sub>3</sub>O<sub>3</sub>S<sub>3</sub> 327.9879, found 327.9876 [M + H]<sup>+</sup>.

389

390 4.4.20. 2-((2-nitrophenyl)disulfanyl)thiazole (**3-20**)

391 Yield 90%; m.p.: 105-107 °C; yellow solid; <sup>1</sup>H NMR (400 MHz, DMSO-*d*<sub>6</sub>), δ 8.37 (d, *J* = 8.2 Hz,  
392 1H, ArH), 8.23 (d, *J* = 8.2 Hz, 1H, ArH), 7.93 (t, *J* = 7.7 Hz, 1H, ArH), 7.87 – 7.74 (m, 2H, CH),  
393 7.62 (t, *J* = 7.7 Hz, 1H, ArH); <sup>13</sup>C NMR (101 MHz, DMSO-*d*<sub>6</sub>), δ 163.8, 145.6, 144.9, 136.2,  
394 133.9, 128.7, 127.6, 126.9, 124.5; HRMS(MALDI) m/z: calculated for C<sub>9</sub>H<sub>6</sub>N<sub>2</sub>O<sub>2</sub>S<sub>3</sub> 270.9664,  
395 found 270.9663 [M+H]<sup>+</sup>.

396

397 4.4.21. 2-(*p*-tolyl)disulfanyl)thiazole (**3-21**)

398 Yield 75%; m.p.: 60-62 °C; yellow solid; <sup>1</sup>H NMR (400 MHz, CDCl<sub>3</sub>), δ 7.80 (d, *J* = 6.1 Hz, 2H,  
399 ArH), 7.53 (d, *J* = 7.9 Hz, 2H, ArH), 7.25 (d, *J* = 7.7 Hz, 2H, ArH), 2.30 (s, 3H, CH<sub>3</sub>); <sup>13</sup>C NMR  
400 (101 MHz, CDCl<sub>3</sub>), δ 136.5, 136.3, 130.2, 129.3, 127.6, 124.9, 21.5; HRMS(MALDI) m/z:  
401 calculated for C<sub>10</sub>H<sub>9</sub>NS<sub>3</sub> 239.9969, found 239.9970 [M+H]<sup>+</sup>.

402

403 4.4.22. 2-((4-fluorophenyl)disulfanyl)thiazole (**3-22**)

404 Yield 82%; m.p.: 89-91 °C; yellow solid; <sup>1</sup>H NMR (400 MHz, DMSO-*d*<sub>6</sub>), δ 8.37 (d, *J* = 8.2 Hz,  
405 1H, ArH), 8.23 (d, *J* = 8.2 Hz, 1H, ArH), δ 7.66 (d, *J* = 8.7 Hz, 2H, ArH), 7.52 (d, *J* = 8.7 Hz, 2H,  
406 ArH); <sup>13</sup>C NMR (101 MHz, DMSO-*d*<sub>6</sub>), δ 144.9, 132.7, 132.6, 130.6, 125.0, 123.9, 117.3, 117.1,  
407 40.1, 39.9, 39.7; HRMS(MALDI) m/z: calculated for C<sub>9</sub>H<sub>6</sub>FNS<sub>3</sub> 243.9719, found 243.9721  
408 [M+H]<sup>+</sup>.

409

410 4.4.23. 2-((4-bromophenyl)disulfanyl)thiazole (**3-23**)

411 Yield 80%; m.p.: 92-94 °C; yellow solid; <sup>1</sup>H NMR (400 MHz, DMSO-*d*<sub>6</sub>), δ 7.61 (d, *J* = 8.5 Hz,  
412 2H, ArH), 7.48 (d, *J* = 8.5 Hz, 2H, ArH), 7.30 (s, 1H, NCH), 6.99 (d, *J* = 4.3 Hz, 1H, SCH); <sup>13</sup>C  
413 NMR (101 MHz, DMSO-*d*<sub>6</sub>), δ 134.9, 132.3, 129.2, 121.9, 114.2, 99.4; HRMS(MALDI) m/z:  
414 calculated for C<sub>9</sub>H<sub>6</sub>BrNS<sub>3</sub> 303.8918, found 303.8914 [M+H]<sup>+</sup>.

415

416 4.4.24. 4-methyl-2-((2-nitrophenyl)disulfanyl)thiazole (**3-24**)

417 Yield 92%; m.p.: 61-63 °C; yellow solid; <sup>1</sup>H NMR (400 MHz, CDCl<sub>3</sub>), δ 8.36 (d, *J* = 8.2 Hz, 1H,  
418 ArH), 8.20 (d, *J* = 8.2 Hz, 1H, ArH), 8.01 – 7.84 (m, 1H, ArH), 7.64 – 7.53 (m, 1H, ArH), 7.33 (s,

419 1H, CH), 2.33 (s, 3H, CH<sub>3</sub>); <sup>13</sup>C NMR (101 MHz, CDCl<sub>3</sub>), δ 162.8, 154.6, 145.7, 136.0, 133.9,  
420 128.7, 127.6, 126.9, 118.4, 17.3; HRMS(MALDI) m/z: calculated for C<sub>10</sub>H<sub>8</sub>N<sub>2</sub>O<sub>2</sub>S<sub>3</sub> 284.9821,  
421 found 284.9823 [M+H]<sup>+</sup>.

422

423 4.4.25. ethyl 2-((4-methylthiazol-2-yl)disulfanyl)benzoate (3-25)

424 Yield 91%; m.p.: 103-105 °C; yellow solid; <sup>1</sup>H NMR (400 MHz, DMSO-*d*<sub>6</sub>), δ 8.09 – 8.03 (m, 1H,  
425 ArH), 8.01 (d, *J* = 7.9 Hz, 1H, ArH), 7.74 (t, *J* = 7.7 Hz, 1H, ArH), 7.45 (t, *J* = 7.5 Hz, 1H, ArH),  
426 7.28 (s, 1H), 4.41 (s, 2H, CH<sub>2</sub>CH<sub>3</sub>), 2.32 (s, 3H, CH<sub>3</sub>), 1.36 (t, *J* = 7.1 Hz, 3H, CH<sub>2</sub>CH<sub>3</sub>); <sup>13</sup>C  
427 NMR (101 MHz, DMSO-*d*<sub>6</sub>), δ 166.2, 156.3, 154.5, 147.4, 138.4, 134.4, 131.8, 127.4, 125.9,  
428 117.6, 62.2, 17.4, 14.5; HRMS(MALDI) m/z: calculated for C<sub>13</sub>H<sub>13</sub>NO<sub>2</sub>S<sub>3</sub> 312.0181, found  
429 312.0188 [M+H]<sup>+</sup>.

430

431 4.4.26. methyl 2-((5-methyl-1,3,4-oxadiazol-2-yl)disulfanyl)benzoate (3-26)

432 Yield 93%; m.p.: 80-82 °C; yellow solid; <sup>1</sup>H NMR (400 MHz, DMSO-*d*<sub>6</sub>), δ 8.14 (d, *J* = 7.4 Hz,  
433 1H, ArH), 8.03 (d, *J* = 6.7 Hz, 1H, ArH), 7.78 (s, 1H, ArH), 7.47 (d, *J* = 6.3 Hz, 1H, ArH), 3.89 (s,  
434 3H, OCH<sub>3</sub>), 2.49 (s, 3H, CH<sub>3</sub>); <sup>13</sup>C NMR (101 MHz, DMSO-*d*<sub>6</sub>), δ 167.3, 166.7, 161.7, 138.7,  
435 134.4, 131.6, 127.4, 127.1, 126.5, 53.3, 11.3; HRMS(MALDI) m/z: calculated for C<sub>11</sub>H<sub>10</sub>N<sub>2</sub>O<sub>3</sub>S<sub>2</sub>  
436 283.0206, found 283.0209 [M+H]<sup>+</sup>.

437

438 4.4.27. ethyl 2-((5-methyl-1,3,4-oxadiazol-2-yl)disulfanyl)benzoate (3-27)

439 Yield 88%; m.p.: 73-74 °C; yellow solid; <sup>1</sup>H NMR (400 MHz, DMSO-*d*<sub>6</sub>), δ 8.14 (d, *J* = 8.0 Hz,  
440 1H, ArH), 8.04 (d, *J* = 7.7 Hz, 1H, ArH), 7.78 (t, *J* = 7.8 Hz, 1H, ArH), 7.46 (t, *J* = 7.5 Hz, 1H,  
441 ArH), 4.35 (q, *J* = 7.1 Hz, 2H, CH<sub>2</sub>CH<sub>3</sub>), 2.50 (s, 3H, CH<sub>3</sub>), 1.34 (t, *J* = 7.1 Hz, 3H, CH<sub>2</sub>CH<sub>3</sub>); <sup>13</sup>C  
442 NMR (101 MHz, DMSO-*d*<sub>6</sub>), δ 167.3, 166.3, 161.7, 138.6, 134.3, 131.6, 127.4, 126.5, 62.2, 14.5,  
443 11.3; HRMS(MALDI) m/z: calculated for C<sub>12</sub>H<sub>12</sub>N<sub>2</sub>O<sub>3</sub>S<sub>2</sub> 297.0362, found 297.0365 [M+H]<sup>+</sup>.

444

445 4.4.28. 2-methyl-5-((2-nitrophenyl)disulfanyl)-1,3,4-oxadiazole (3-28)

446 Yield 92%; m.p.: 91-93 °C; yellow solid; <sup>1</sup>H NMR (400 MHz, DMSO-*d*<sub>6</sub>), δ 8.34 (d, *J* = 8.2 Hz,  
447 1H, ArH), 8.30 (d, *J* = 8.2 Hz, 1H, ArH), 7.97 (t, *J* = 7.7 Hz, 1H, ArH), 7.63 (t, *J* = 7.7 Hz, 1H,  
448 ArH), 2.51 (s, 3H, CH<sub>3</sub>); <sup>13</sup>C NMR (101 MHz, DMSO-*d*<sub>6</sub>), δ 167.5, 161.2, 145.4, 135.9, 134.0,  
449 128.7, 128.1, 126.8, 11.3; HRMS(MALDI) m/z: calculated for C<sub>9</sub>H<sub>7</sub>N<sub>3</sub>O<sub>3</sub>S<sub>2</sub> 270.0002, found  
450 270.0000 [M+H]<sup>+</sup>.

451

452 4.4.29. methyl 2-((1,3,4-oxadiazol-2-yl)disulfanyl)benzoate (3-29)

453 Yield 87%; m.p.: 99-101 °C; yellow solid; <sup>1</sup>H NMR (400 MHz, DMSO-*d*<sub>6</sub>), δ 9.37 (s, 1H, CH),  
454 8.14 (d, *J* = 8.2, Hz, 1H, ArH), 8.05 (d, *J* = 7.8, Hz, 1H, ArH), 7.87 (t, *J* = 7.8, Hz, 1H, ArH), 7.48  
455 (t, *J* = 7.7, Hz, 1H, ArH), 3.91 (s, 3H, OCH<sub>3</sub>); <sup>13</sup>C NMR (101 MHz, DMSO-*d*<sub>6</sub>), δ 166.8, 162.3,  
456 157.5, 138.5, 134.5, 131.7, 127.5, 127.2, 126.6, 53.3; HRMS(MALDI) m/z: calculated for

457  $C_{10}H_8N_2O_3S_2$  290.9869, found 290.9868 [M+H]<sup>+</sup>.

458

459 4.4.30. methyl 2-((4-methyloxazol-2-yl)disulfanyl)benzoate (3-30)

460 Yield 90%; m.p.: 68-70 °C; yellow solid; <sup>1</sup>H NMR (400 MHz, DMSO-*d*<sub>6</sub>), δ 8.16 (d, *J* = 8.0 Hz,  
461 1H, ArH), 8.04 (d, *J* = 7.7, Hz, 1H, ArH), 7.97 (s, 1H, CH), 7.88(t, *J* = 7.2 Hz, 1H, ArH), 7.45 (t, *J*  
462 = 7.2 Hz, 1H, ArH), 3.90 (s, 3H, OCH<sub>3</sub>), 2.07 (s 3H, CH<sub>3</sub>); <sup>13</sup>C NMR (101 MHz, DMSO-*d*<sub>6</sub>), δ  
463 166.7, 139.6, 139.3, 138.8, 134.3, 131.6, 127.2, 126.9, 126.4, 53.2, 11.7; HRMS(MALDI) m/z:  
464 calculated for C<sub>12</sub>H<sub>11</sub>NO<sub>3</sub>S<sub>2</sub> 282.0253, found 282.0257 [M+H]<sup>+</sup>.

465

466 4.4.31. 2-((4-chlorophenyl)disulfanyl)-1,3,4-oxadiazole (3-31)

467 Yield 90%; m.p.: 69-72 °C; yellow solid; <sup>1</sup>H NMR (400 MHz, DMSO-*d*<sub>6</sub>), δ 9.46 (s, 1H, CH), 7.71  
468 (d, *J* = 8.5 Hz, 2H, ArH), 7.54 (d, *J* = 8.3 Hz, 2H, ArH); <sup>13</sup>C NMR (101 MHz, DMSO-*d*<sub>6</sub>), δ 157.7,  
469 134.7, 133.8, 132.5, 131.4, 130.1; HRMS(MALDI) m/z: calculated for C<sub>8</sub>H<sub>5</sub>ClN<sub>2</sub>O<sub>2</sub>S<sub>2</sub> 261.9871,  
470 found 261.9872 [M + NH<sub>4</sub>]<sup>+</sup>.

471

472 4.4.32. 4,6-dimethyl-2-((2-nitrophenyl)disulfanyl)pyrimidine (3-32)

473 Yield 94%; m.p.: 151-153 °C; yellow solid; <sup>1</sup>H NMR (400 MHz, DMSO-*d*<sub>6</sub>), δ 8.34 (d, 6.5 Hz, 1H,  
474 ArH), 7.99 – 7.69 (m, 2H, ArH), 7.55 (d, *J* = 8.4 Hz, 1H, ArH), 7.12 (d, *J* = 25.8 Hz, 1H, ArH),  
475 2.35 (s, 6H, CH<sub>3</sub>); <sup>13</sup>C NMR (101 MHz, DMSO-*d*<sub>6</sub>), δ 168.7, 168.3, 135.5, 128.5, 128.0, 127.4,  
476 127.0, 126.3, 118.7, 118.1, 23.8; HRMS(MALDI) m/z: calculated for C<sub>12</sub>H<sub>11</sub>N<sub>3</sub>O<sub>2</sub>S<sub>2</sub> 294.0365,  
477 found 294.0364 [M + H]<sup>+</sup>.

478

479 4.4.33. 2-((4-chlorophenyl)disulfanyl)-4,6-dimethylpyrimidine (3-33)

480 Yield 80%; m.p.: 84-86 °C; yellow solid; <sup>1</sup>H NMR (400 MHz, DMSO-*d*<sub>6</sub>), δ 7.60 (d, *J* = 8.6 Hz,  
481 2H, ArH), 7.44 (d, *J* = 8.6 Hz, 2H, ArH), 7.14 (s, 1H, ArH), 2.40 (s, 6H, CH<sub>3</sub>); <sup>13</sup>C NMR (101  
482 MHz, DMSO-*d*<sub>6</sub>), δ 168.6, 167.8, 135.6, 133.1, 130.9, 129.6, 118.4, 23.8; HRMS(MALDI) m/z:  
483 calculated for C<sub>12</sub>H<sub>11</sub>ClN<sub>2</sub>S<sub>2</sub> 283.0125, found 283.0130 [M + H]<sup>+</sup>.

484

485 4.4.34. 2-((4-bromophenyl)disulfanyl)-4,6-dimethylpyrimidine (3-34)

486 Yield 84%; m.p.: 76-79 °C; yellow solid; <sup>1</sup>H NMR (400 MHz, DMSO-*d*<sub>6</sub>), δ 7.53 (dd, *J* = 15.6, 7.2  
487 Hz, 4H, ArH), 7.15 (s, 1H, ArH), 2.38 (s, 6H, CH<sub>3</sub>); <sup>13</sup>C NMR (101 MHz, DMSO-*d*<sub>6</sub>), δ 168.6,  
488 167.7, 136.1, 132.5, 131.0, 121.5, 118.4, 23.8; HRMS(MALDI) m/z: calculated for C<sub>12</sub>H<sub>11</sub>BrN<sub>2</sub>S<sub>2</sub>  
489 326.9620, found 326.9622 [M + H]<sup>+</sup>.

490

491 4.4.35. 4,6-dimethyl-2-(phenyldisulfanyl)pyrimidine (3-35)

492 Yield 81%; m.p.: 61-63 °C; yellow solid; <sup>1</sup>H NMR (400 MHz, DMSO-*d*<sub>6</sub>), δ 7.67 (t, *J* = 8.0 Hz, 2H,  
493 ArH), 7.60 – 7.31 (m, 3H, ArH), 7.22 (s, 1H, ArH), 2.48 (s, 6H, CH<sub>3</sub>); <sup>13</sup>C NMR (101 MHz,  
494 DMSO-*d*<sub>6</sub>), δ 168.6, 130.9, 129.7, 129.6, 129.2, 128.3, 118.4, 23.8; HRMS(MALDI) m/z:  
495 calculated for C<sub>12</sub>H<sub>12</sub>N<sub>2</sub>S<sub>2</sub> 249.0515, found 249.0515 [M + H]<sup>+</sup>.

496

497 4.4.36. 4,6-dimethyl-2-(*p*-tolylidisulfanyl)pyrimidine (3-36)

498 Yield 84%; m.p.: 72-75 °C; yellow solid; <sup>1</sup>H NMR (400 MHz, DMSO-*d*<sub>6</sub>), δ 7.50 (d, *J* = 8.2 Hz,  
499 2H, ArH), 7.18 (d, *J* = 8.0 Hz, 2H, ArH), 7.12 (s, 1H, ArH), 2.40 (s, 6H, CH<sub>3</sub>), 2.28 (s, 3H, CH<sub>3</sub>);  
500 <sup>13</sup>C NMR (101 MHz, DMSO-*d*<sub>6</sub>), δ 168.4, 138.4, 133.1, 131.6, 130.3, 130.2, 118.2, 23.86, 21.1;  
501 HRMS(MALDI) *m/z*: calculated for C<sub>13</sub>H<sub>14</sub>N<sub>2</sub>S<sub>2</sub> 263.0671, found 263.0674 [M + H]<sup>+</sup>.

502

## 503 4.4.37. 2-((2-nitrophenyl)disulfanyl)pyrimidine (3-37)

504 Yield 86%; m.p.: 130-132 °C; yellow solid; <sup>1</sup>H NMR (400 MHz, DMSO-*d*<sub>6</sub>), δ 8.63 (s, 2H, ArH),  
505 8.31 (d, *J* = 8.1 Hz, 2H, ArH), 7.96 (s, 1H, ArH), 7.59 (s, 1H, ArH), 7.38 (s, 1H, ArH), 7.17 (s, 1H,  
506 ArH); <sup>13</sup>C NMR (101 MHz, DMSO-*d*<sub>6</sub>), δ 169.4, 158.6, 136.3, 134.3, 128.1, 126.7, 125.9, 118.9,  
507 99.9; HRMS(MALDI) *m/z*: calculated for C<sub>10</sub>H<sub>7</sub>N<sub>3</sub>O<sub>2</sub>S<sub>2</sub> 265.0052, found 266.0053 [M + H]<sup>+</sup>.

508

## 509 4.4.38. 2-((4-chlorophenyl)disulfanyl)pyrimidine (3-38)

510 Yield 80%; m.p.: 79-80 °C; yellow solid; <sup>1</sup>H NMR (400 MHz, DMSO-*d*<sub>6</sub>), δ 8.66 – 8.47 (m, 2H),  
511 7.47 (t, *J* = 9.0 Hz, 2H), 7.29 – 7.16 (m, 2H), 7.07 (d, *J* = 4.9 Hz, 1H); <sup>13</sup>C NMR (101 MHz,  
512 DMSO-*d*<sub>6</sub>), δ 158.0, 134.9, 133.8, 130.2, 129.3, 129.1, 118.3; HRMS(MALDI) *m/z*: calculated for  
513 C<sub>10</sub>H<sub>7</sub>ClN<sub>2</sub>S<sub>2</sub> 254.9812, found 254.9816 [M + H]<sup>+</sup>.

514

515

## 516 4.4.39. 2-((4-bromophenyl)disulfanyl)pyrimidine (3-39)

517 Yield 83%; m.p.: 75-78 °C; yellow solid; <sup>1</sup>H NMR (400 MHz, DMSO-*d*<sub>6</sub>), δ 8.63 (dd, *J* = 22.9, 4.7  
518 Hz, 2H), 7.43 (dd, *J* = 20.0, 12.8 Hz, 4H), 7.10 (d, *J* = 4.0 Hz, 1H); <sup>13</sup>C NMR (101 MHz,  
519 DMSO-*d*<sub>6</sub>), δ 158.1, 135.5, 132.0, 130.3, 128.9, 121.8, 118.3; HRMS(MALDI) *m/z*: calculated for  
520 C<sub>10</sub>H<sub>7</sub>BrN<sub>2</sub>S<sub>2</sub> 298.9307, found 298.9307 [M + H]<sup>+</sup>.

521

522 4.4.40. 2-(*p*-tolylidisulfanyl)pyrimidine (3-40)

523 Yield 86%; m.p.: 45-48 °C; yellow solid; <sup>1</sup>H NMR (400 MHz, DMSO-*d*<sub>6</sub>), δ 8.56 (d, *J* = 4.9 Hz,  
524 2H), 7.44 (d, *J* = 8.2 Hz, 2H), 7.13 – 6.90 (m, 3H), 2.24 (s, 3H, CH<sub>3</sub>); <sup>13</sup>C NMR (101 MHz,  
525 DMSO-*d*<sub>6</sub>), δ 171.2, 157.9, 138.1, 132.9, 129.8, 129.7, 118.0, 21.1; HRMS(MALDI) *m/z*:  
526 calculated for C<sub>11</sub>H<sub>10</sub>N<sub>2</sub>S<sub>2</sub> 235.0358, found 235.0361 [M + H]<sup>+</sup>.

527

528 4.5. *In vitro* Enzyme inhibition assay

529 The expression and purification of SARS CoV M<sup>pro</sup> was described by Rao et al [42]. Basically,  
530 the sequence of SARS-CoV M<sup>pro</sup> cloned into the pGEX-6P-1 vector was transformed into *E. coli*  
531 BL21 (DE3) cells. The GST fusion protein, GST-SARS-CoV M<sup>pro</sup>, was purified by  
532 GST-glutathione affinity chromatography, cleaved with PreScission protease, and the recombinant  
533 SARS-CoV M<sup>pro</sup> was further purified by using anion-exchange chromatography. Eventually  
534 purified protein was of high purity (>95%) as judged by SDS-PAGE analysis and the

535 concentration is 0.5  $\mu\text{M}$ , and the buffer contains 50 mM Tris-HCl, pH 7.3 and 1 mM EDTA. The  
 536 fluorogenic substrate with consensus sequence of CoV M<sup>pro</sup>,  
 537 MCA-AVLQSGFR-Lys(Dnp)-Lys-NH<sub>2</sub> (95% purity), was synthesized in Shanghai Biological  
 538 Engineering Company. The substrate was dissolved in DMSO in 0.8 mM liquid storage for use.

539

540 The inhibition assay was similar to Yang's procedure [11]. The SARS CoV M<sup>pro</sup> inhibition assays  
 541 were conducted by fluorescence resonance energy transfer (FRET). The natural substrate amino  
 542 acid sequence (AVLQSGFRKK) of SARS-CoV M<sup>pro</sup> started with the MCA fluorescent group and  
 543 connected the Dnp fluorescence quenching group with penultimate K. The tested compounds were  
 544 dissolved by sterilized DMSO and diluted to various concentrations. The settled concentrations of  
 545 proteins, compounds and substrate were preheated at 37 °C and oscillated. The excitation/emission  
 546 light was 320/405 nm, and the test was carried out every 5 s for 200 times. Drawing curves, the  
 547 maximum value of the negative control curve slope is  $V_0$ , and the largest compound curve slope is  
 548  $V_1$ . The inhibition ratio can be defined  $(1-V_1/V_0)$ . And the  $IC_{50}$  value was calculated by equation  
 549 (1) using GraphPad Prism5:

$$550 \quad V_0/V = 1 + [I]/IC_{50} \quad (1)$$

551  $V_0$  shows the initial rate of the reaction without inhibitor,  $V$  means the initial rate of the reaction  
 552 with the inhibitor at various concentrations and  $[I]$  indicates the concentration of the inhibitor.

553

554 The determination of the inhibitor as a valent inhibitor employs the above methods as well, albeit  
 555 with two modifications. Firstly, the inhibitor concentration was set to 2 or 4  $\mu\text{M}$ . And for each  
 556 inhibitor concentration, we measured the enzymatic activity of M<sup>pro</sup> whose concentration spans 0  
 557 to 2  $\mu\text{M}$ . Secondly, M<sup>pro</sup> and inhibitor were first incubated for 20 min to ensure a thorough  
 558 'M<sup>pro</sup>-inhibitor' reaction and then the inhibition assay was initiated by adding substrate and  
 559 characterized by fluorescence monitoring.

560

561 The further characterization of the inhibitor as a non-competitive inhibitor employs the methods  
 562 described in earlier work [28]. Basically, the enzymatic velocity of SARS-CoV M<sup>pro</sup> versus  
 563 substrate concentrations with presence of inhibitors is depicted by equation (2) [27], where  $K_i$  is  
 564 the dissociation constant for the SARS-CoV M<sup>pro</sup> complexed with inhibitor **3-31**; factor  $\alpha$  reflects  
 565 the effect of inhibitor **3-31** on the affinity of the enzyme for its substrate;  $V_{\max}$  and  $K_m$  represent  
 566 the maximum velocity and Michaelis-Menten constant, respectively.

$$567 \quad v = \frac{V_{\max} [S]}{[S] \left( 1 + \frac{[I]}{\alpha K_i} \right) + K_m \left( 1 + \frac{[I]}{K_i} \right)} \quad (2)$$

568 The values of  $V_{\max}$  and  $K_m$  at different inhibitor concentrations were apparent  $V_{\max}$  and  $K_m$ , called  
 569  $V_{\max}^{app}$  and  $K_m^{app}$ , respectively. According to equation (2),  $V_{\max}^{app}$  and  $K_m^{app}$  can be calculated by  
 570 equation (3).

$$V_{\max}^{app} = \frac{V_{\max}}{1 + \frac{[I]}{\alpha K_i}}, K_m^{app} = \frac{K_m \left(1 + \frac{[I]}{K_i}\right)}{1 + \frac{[I]}{\alpha K_i}} \quad (3)$$

571

572 The kinetic parameters of  $V_{\max}^{app}$  and  $K_m^{app}$ , were determined by adding 1 $\mu$ M SARS-CoV M<sup>pro</sup> to  
 573 20 $\mu$ M substrate containing varying concentrations of inhibitor 3-31 (0-3 $\mu$ M). The value of  $\alpha K_i$   
 574 was then calculated from plots of  $1/V_{\max}^{app}$  versus  $1/[I]$ . Similarly, the value of  $K_i$  was calculated  
 575 from plots of  $V_{\max}^{app}$  and  $K_m^{app}$  versus  $1/[I]$ .

576

577 Mass spectra were recorded on Waters Xevo G2-XS Q-TOF mass spectrometry. Mass spectra  
 578 were acquired in positive ion mode using a capillary voltage of 3 kV, a sampling cone voltage of  
 579 40 V and a source offset voltage of 80 V. The cone gas flow was set up to 50 L/h and desolvation  
 580 gas flow was 800 L/h. Desolvation temperature and source temperature were set to 400 °C and  
 581 100 °C, respectively. The mass of intact protein was obtained by deconvolution of the raw data  
 582 using MaxEnt1 tool. The samples were prepared at the similar condition with the  $IC_{50}$   
 583 determination, except that the concentration of the inhibitors was 20 times of the concentration of  
 584 SARS M<sup>pro</sup>.

585

#### 586 4.6 Molecular docking and comparative field analysis

587 Chemical structures of the compounds were built within Sybyl 7.3 (Tripos Inc., St Louis, MO).  
 588 All the molecules were assigned Gasteiger-Hückel charges and minimized by the Tripos force  
 589 field when convergence reached 0.001 kcal/mol/Å.

590

591 Molecular docking of the unsymmetrical aromatic disulfides to the active site of SARS-CoV M<sup>pro</sup>  
 592 was performed by FlexX. The crystal structure of SARS-CoV M<sup>pro</sup> in complex with inhibitor (pdb  
 593 code 2AMD) was retrieved from the pdb databank. All water molecules were removed, and  
 594 hydrogen atoms were added in the standard geometry. Any amino acid residue within 6.5 Å of the  
 595 location of the original inhibitor N9 was considered to be in the binding pocket. Cscore calculation  
 596 was enabled and set to serial mode. Database docking and subsequent scoring procedures were  
 597 performed using the default parameters in the program.

598

599 For CoMFA, The molecules were superimposed using **3-31** from the molecular docking result as  
 600 the template. All the parameters were used the default value within CoMFA module and the  
 601 column filtering was set to 2.0 kcal/mol. The “leave-one-out” (LOO) cross validation method was  
 602 applied to determine the optimum number of partial least squares (PLS) components. The  
 603 non-cross validated method was used to derive the final model to explain the quantitative  
 604 structure-activity relationship in a three dimensional manner.

605

606 **Acknowledgment**

607 This work was financially supported by the Natural Science Foundation of China (No. 21272128  
608 and 21672114), the “111” Project of Ministry of Education of China (No. B06005) and the  
609 National Basic Research Program of China (No. 2013CB734004). We appreciate Professor  
610 Chuanzheng Zhou in Nankai University for his kind assistance for the mass spectrometry of SARS  
611 CoV main protease.

612

613 **Appendix A. Supplementary data**

614 Supplementary data related to this article can be found at <http://dx.doi.org/XXXXXX>

615

616

617

618

619

620

621

622

623

624

625

626

627

628

629

630

631

632

633

634

635

636 **References**

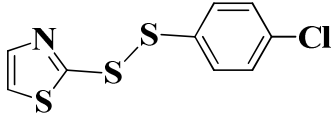
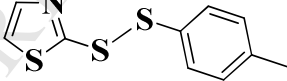
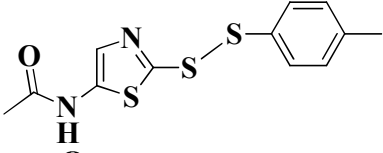
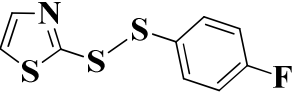
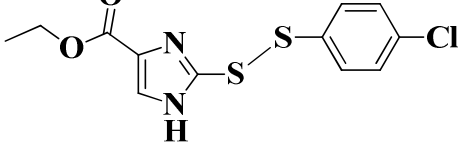
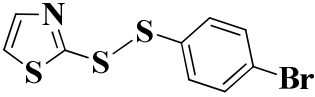
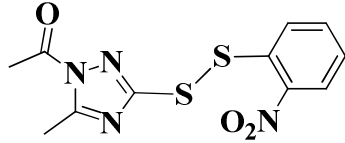
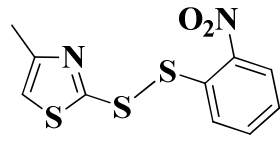
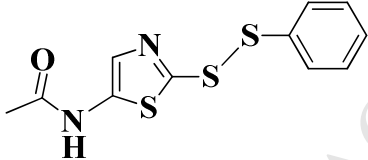
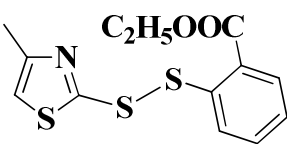
- 637 [1] World Health Organization. Summary of probable SARS cases with onset of illness from 1  
638 November 2002 to 31 July 2003 Based on data as of the 31 December 2003.  
639 [http://www.who.int/csr/sars/country/table2004\\_04\\_21/en/](http://www.who.int/csr/sars/country/table2004_04_21/en/)
- 640 [2] D.H. Goetz, Y. Choe, E. Hansell, Y.T. Chen, M. McDowell, C.B. Jonsson, W.R. Roush, J.  
641 McKerrow, C.S. Craik. Substrate specificity profiling and identification of a new class of  
642 inhibitor for the major protease of the SARS coronavirus, *Biochemistry* 46 (2007)  
643 8744-8752.
- 644 [3] H. Yang, W. Xie, X. Xue, K. Yang, J. Ma, W. Liang, Q. Zhao, Z. Zhou, D. Pei, J. Ziebuhr, R.  
645 Hilgenfeld, K.Y. Yuen, L. Wong, G. Gao, S. Chen, Z. Chen, D. Ma, M. Bartlam, Z. Rao.  
646 Design of wide-spectrum inhibitors targeting coronavirus main proteases, *PLoS Biol.* 3 (2005)  
647 1741-1752.
- 648 [4] K. Anand, J. Ziebuhr, P. Wadhvani, J.R. Mesters, R. Hilgenfeld. Coronavirus main proteinase  
649 (3CL<sup>pro</sup>) structure: basis for design of anti-SARS drugs. *Science* 300 (2003) 1763-1767.
- 650 [5] L. Zhou, Y. Liu, W. Zhang, P. Wei, C. Huang, J. Pei, Y. Yuan, L. Lai. Isatin compounds as  
651 non-covalent SARS coronavirus 3C-like protease inhibitors. *J. Med. Chem.* 49 (2006)  
652 3440-3443.
- 653 [6] L. Chen, J. Li, C. Luo, H. Liu, W. Xu, G. Chen, O.W. Liew, W. Zhu, C.M. Puah, X. Shen, H.  
654 Jiang. Binding interaction of quercetin-3- $\beta$ -galactoside and its synthetic derivatives with  
655 SARS-CoV 3CL<sup>pro</sup>: structure-activity relationship studies reveal salient pharmacophore  
656 features. *Bioorg. Med. Chem.* 14 (2006) 8295-8306.
- 657 [7] R. Ramajayam, K.P. Tan, H.G. Liu, P.H. Liang. Synthesis and evaluation of pyrazolone  
658 compounds as SARS-coronavirus 3C-like protease inhibitors. *Bioorg. Med. Chem.* 18 (2010)  
659 7849-7854.
- 660 [8] Y.M. Shao, W.B. Yang, T.H. Kuo, K.C. Tsai, C.H. Lin, A.S. Yang, P.H. Liang, C.H. Wong.  
661 Design, synthesis, and evaluation of trifluoromethyl ketones as inhibitors of SARS-CoV 3CL  
662 protease. *Bioorg. Med. Chem.* 16 (2008) 4652-4660.
- 663 [9] J. Jacobs, V. Grum-Tokars, Y. Zhou, M. Turlington, S.A. Saldanha, P. Chase, A. Egger, E.S.  
664 Dawson, Y.M. Baez-Santos, S. Tomar, A.M. Mielech, S.C. Baker, C.W. Lindsley, P. Hodder,  
665 A. Mesecar, S.R. Stauffer. Discovery, synthesis, and structure-based optimization of a series  
666 of N-(tert-butyl)-2-(N-arylamido)-2-(pyridin-3-yl) acetamides (ML188) as potent  
667 non-covalent small molecule inhibitors of the severe acute respiratory syndrome coronavirus  
668 (SARS-CoV) 3CL protease. *J. Med. Chem.* 56 (2013) 534-546.
- 669 [10] P. Thanigaimalai, S. Konno, T. Yamamoto, Y. Koiwai, A. Taguchi, K. Takayama, F. Yakushiji,  
670 K. Akaji, S.E. Chen, A. Naser-Tavakolian, A. Schön, E. Freire, Y. Hayashi. Development of  
671 potent dipeptide-type SARS-CoV 3CL protease inhibitors with novel P3 scaffolds: design,  
672 synthesis, biological evaluation, and docking studies. *Eur. J. Med. Chem.* 68 (2013) 372-384.
- 673 [11] W. Liu, H.M. Zhu, G.J. Niu, E.Z. Shi, J. Chen, B. Sun, W.Q. Chen, H.G. Zhou, C. Yang.

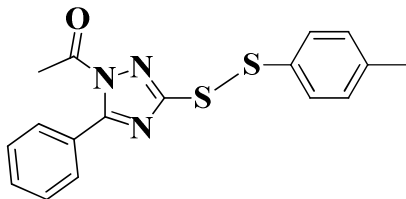
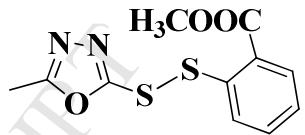
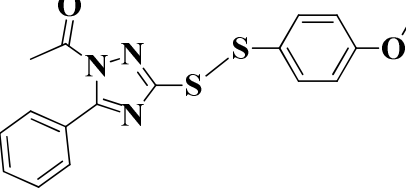
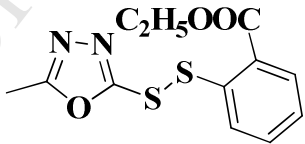
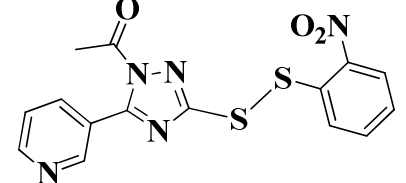
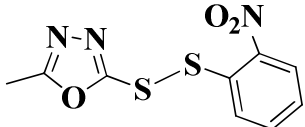
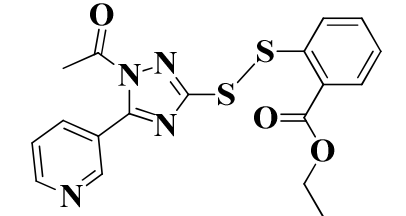
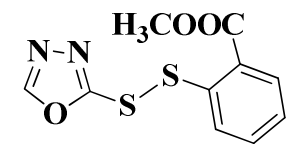
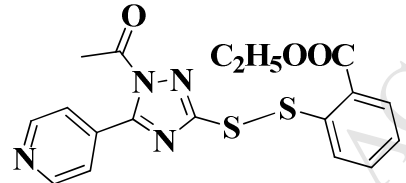
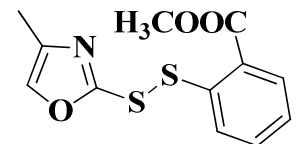
- 674 Synthesis, modification and docking studies of 5-sulfonyl isatin derivatives as SARS-CoV  
675 3C-like protease inhibitors. *Bioorg. Med. Chem.* 22 (2014) 292-302.
- 676 [12] P. Thanigaimalai, S. Konno, T. Yamamoto, Y. Koiwai, A. Taguchi, K. Takayama, F. Yakushiji,  
677 K. Akaji, Y. Kiso, Y. Kawasaki, S.E. Chen, A. Naser-Tavakolian, A. Schön, E. Freire, Y.  
678 Hayashi. Design, synthesis, and biological evaluation of novel dipeptide-type SARS-CoV  
679 3CL protease inhibitors: structure-activity relationship study. *Eur. J. Med. Chem.* 65 (2013)  
680 436-447.
- 681 [13] L. Zhang, C.P. Chou, M. Moo-Young. Disulfide bond formation and its impact on the  
682 biological activity and stability of recombinant therapeutic proteins produced by *Escherichia*  
683 *coli* expression system. *Biotechnol. Adv.* 29 (2011) 923-929.
- 684 [14] R. Argüello-García, O.N. Medina-Campos, N. Pérez-Hernández, J. Pedraza-Chaverrí, G.  
685 Ortega-Pierres. Hypochlorous acid scavenging activities of thioallyl compounds from garlic.  
686 *J. Agric. Food Chem.* 58 (2010) 11226–11233.
- 687 [15] H.L. Chu, B.S. Wang, P.D. Duh. Effects of selected organosulfur compounds on melanin  
688 formation. *J. Agric. Food Chem.* 57 (2009) 7072–7077.
- 689 [16] S. Otto. Dynamic molecular networks: from synthetic receptors to self-replicators. *Acc.*  
690 *Chem. Res.* 45 (2012) 2200-2210.
- 691 [17] E. Turos, K.D. Revell, P. Ramaraju, D.A. Gergeres, K. Greenhalgh, A. Young, N.  
692 Sathyanarayan, S. Dickey, D. Lim, M.M. Alhamadsheh, K. Reynolds. Unsymmetric  
693 aryl-alkyl disulfide growth inhibitors of methicillin-resistant *Staphylococcus aureus* and  
694 *Bacillus anthracis*. *Bioorg. Med. Chem.* 16 (2008) 6501-6508.
- 695 [18] T.R. DiRaimondo, N.M. Plugis, X. Jin, C. Khosla. Selective inhibition of extracellular  
696 thioredoxin by asymmetric disulfides. *J. Med. Chem.* 56 (2013) 1301-1310.
- 697 [19] K.J. Choi, Y.G. Yu, H.G. Hahn, J.D. Choi, M.Y. Yoon. Characterization of acetohydroxyacid  
698 synthase from *Mycobacterium tuberculosis* and the identification of its new inhibitor from  
699 the screening of a chemical library. *FEBS Lett.* 579 (2005) 4903-4910.
- 700 [20] K.J. Choi, K.M. Noh, D.E. Kim, B.H. Ha, E.E. Kim, M.Y. Yoon. Identification of the  
701 catalytic subunit of acetohydroxyacid synthase in *Haemophilus influenzae* and its potent  
702 inhibitors. *Arch. Biochem. Biophys.* 466 (2007) 24-30.
- 703 [21] J. Shang, W.M. Wang, Y.H. Li, H.B. Song, Z.M. Li, J.G. Wang. Synthesis, crystal structure,  
704 in vitro acetohydroxyacid synthase inhibition, in vivo herbicidal activity, and 3D-QSAR of  
705 new asymmetric aryl disulfides. *J. Agric. Food Chem.* 60 (2012) 8286-8293.
- 706 [22] Z.S. Li, W.M. Wang, W. Lu, C.W. Niu, Y.H. Li, Z.M. Li, J.G. Wang. Synthesis and biological  
707 evaluation of nonsymmetrical aromatic disulfides as novel inhibitors of acetohydroxyacid  
708 synthase. *Bioorg. Med. Chem. Lett.* 23 (2013) 3723-3727.
- 709 [23] C.S. Sepúlveda, C.C. García, J.M. Levingston Macleod, N. López, E.B. Damonte. Targeting  
710 of arenavirus RNA synthesis by a carboxamide-derivatized aromatic disulfide with virucidal  
711 activity. *PLoS One.* 8 (2013) e81251.

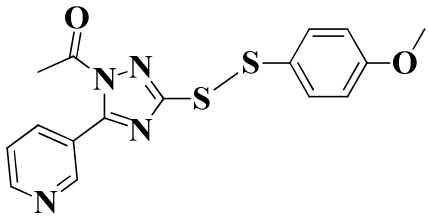
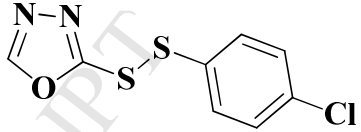
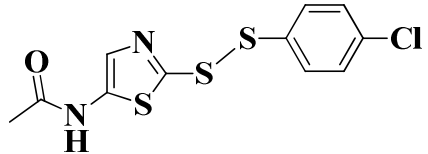
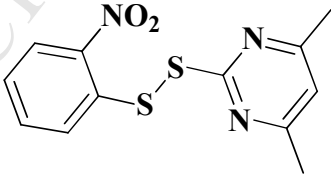
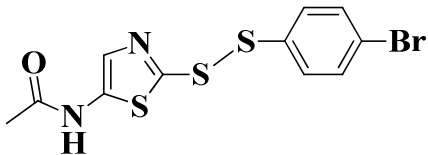
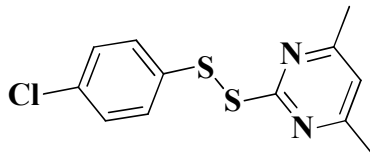
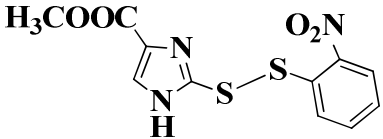
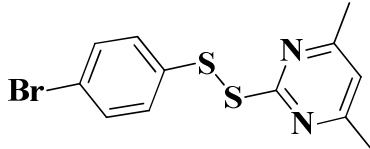
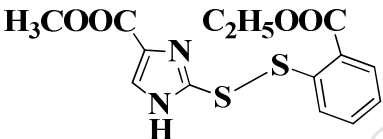
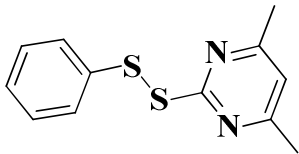
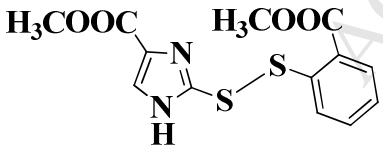
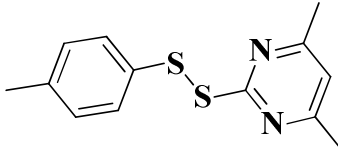
- 712 [24] H.H. Lara, L. Ixtapan-Turrent, E.N. Garza-Treviño, S.M. Flores-Teviño, G. Borkow, C.  
713 Rodriguez-Padilla. Antiviral properties of 5, 5'-dithiobis-2- nitrobenzoic acid and bacitracin  
714 against T-tropic human immunodeficiency virus type 1. *Viol. J.* 8 (2011) 137.
- 715 [25] C.C. García, I. Topisirovic, M. Djavani, K.L. Borden, E.B. Damonte, M.S. Salvato. An  
716 antiviral disulfide compound blocks interaction between arenavirus Z protein and cellular  
717 promyelocytic leukemia protein. *Biochem. Biophys. Res. Commun.* 393 (2010) 625-630.
- 718 [26] M. Han, J.T. Lee, H.G. Hahn, A traceless, one-pot preparation of unsymmetric disulfides  
719 from symmetric disulfides through a repeated process involving sulfenic acid and  
720 thiosulfinate intermediates. *Tetrahedron. Lett.* 52 (2011) 236-239.
- 721 [27] R. Copeland. Reversible inhibitors. In: R. Copeland, *Enzymes: a practical introduction to*  
722 *structure, mechanism, and data analysis.* 2nd ed. New York: Wiley-VCH, Inc. (2000)  
723 266-304.
- 724 [28] F. Wang, C. Chen, X. Liu, K. Yang, X. Xu, H. Yang. Crystal structure of feline infectious  
725 peritonitis virus main protease in complex with synergetic dual inhibitors. *J. Virol.* 90 (2015)  
726 1910-1917.
- 727 [29] P.T. Corbett, J. Leclaire, L. Vial, K.R. West, J.L. Wietor, J.K. Sanders, S. Otto. Dynamic  
728 combinatorial chemistry. *Chem. Rev.* 106 (2006) 3652-3711.
- 729 [30] T. Christopeit, A. Albert, H.K. Leiros. Discovery of a novel covalent non- $\beta$ -lactam inhibitor  
730 of the metallo- $\beta$ -lactamase NDM-1. *Bioorg. Med. Chem.* 24 (2016) 2947-2953.
- 731 [31] J. Zhang, H.I. Pettersson, C. Huitema, C. Niu, J. Yin, M.N. James, L.D. Eltis, J.C. Vederas.  
732 Design, synthesis, and evaluation of inhibitors for severe acute respiratory syndrome 3C-like  
733 protease based on phthalhydrazide ketones or heteroaromatic esters. *J. Med. Chem.* 50 (2007)  
734 1850-1864.
- 735 [32] M. Rarey, B. Kramer, T. Lengauer, G. Klebe, A fast flexible docking method using an  
736 incremental construction algorithm. *J. Mol. Biol.* 261 (1996) 470-489.
- 737 [33] J. Wang, H. Tan, Y. Li, Y. Ma, Z. Li, L.W. Guddat. Chemical synthesis, in vitro  
738 acetoxyacid synthase (AHAS) inhibition, herbicidal activity, and computational studies  
739 of isatin derivatives. *J. Agric. Food Chem.* 59 (2011) 9892-9900.
- 740 [34] G. Jug, M. Anderluh, T. Tomašič. Comparative evaluation of several docking tools for  
741 docking small molecule ligands to DC-SIGN. *J. Mol. Model.* 21 (2015) 164.
- 742 [35] R.K. Mishra, J. Singh. A Structure Guided QSAR: A Rapid and Accurate technique to predict  
743  $IC_{50}$ : A Case Study. *Curr. Comput. Aided Drug Des.* 11 (2015) 152-163.
- 744 [36] H. Liu, Q. Shen, J. Zhang, W. Fu. Evaluation of various inverse docking schemes in multiple  
745 targets identification. *J. Mol. Graph. Model.* 29 (2010) 326-330.
- 746 [37] X. Hou, J. Du, J. Zhang, L. Du, H. Fang, M. Li. How to improve docking accuracy of  
747 AutoDock4.2: a case study using different electrostatic potentials. *J. Chem. Inf. Model.* 2013  
748 Jan 28;53(1):188-200.
- 749 [38] A.C. Wallace, R.A. Laskowski, J.M. Thornton. LIGPLOT: a program to generate schematic

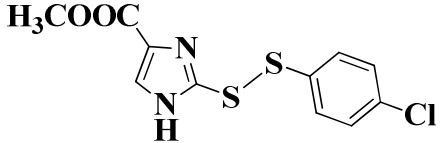
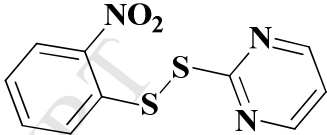
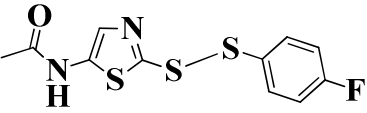
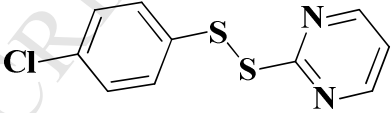
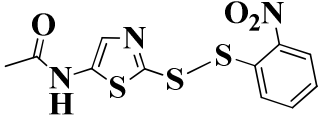
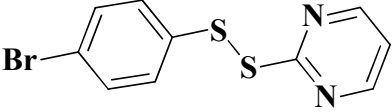
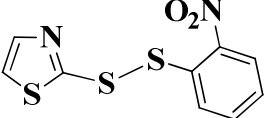
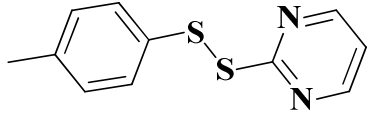
- 750 diagrams of protein-ligand interactions. *Protein Eng.* 8 (1995) 127-134.
- 751 [39] R.D. Cramer, D.E. Patterson, J.D. Bunce, Comparative molecular field analysis (CoMFA). 1.  
752 Effect of shape on binding of steroids to carrier proteins. *J. Am. Chem. Soc.* 110 (1988)  
753 5959-5967.
- 754 [40] D.P. Jiang, C.C. Zhu, X.S. Shao, J.G. Cheng, Z. Li. Bioactive conformation analysis of  
755 anthranilic diamide insecticides: DFT-based potential energy surface scanning and 3D-QSAR  
756 investigations. *Chin. Chem. Lett.* 26 (2015) 662-666.
- 757 [41] X.L. Yue, H. Li, S.S. Liu, Q.Y. Zhang, J.J. Yao, F.Y. Wang. N-Fluorinated  
758 phenyl-N'-pyrimidyl urea derivatives: Synthesis, biological evaluation and 3D-QSAR study.  
759 *Chin. Chem. Lett.* 25 (2014) 1069-1072.
- 760 [42] C.A. Lipinski, F. Lombardo, B.W. Dominy, P.J. Feeney. Experimental and computational  
761 approaches to estimate solubility and permeability in drug discovery and development  
762 settings. *Adv. Drug Deliv. Rev.* 46 (2001) 3-26.
- 763 [43] H. Yang, M. Yang, Y. Ding, Y. Liu, Z. Lou, Z. Zhou, L. Sun, L. Mo, S. Ye, H. Pang, G.F. Gao,  
764 K. Anand, M. Bartlam, R. Hilgenfeld, Z. Rao. The crystal structures of severe acute  
765 respiratory syndrome virus main protease and its complex with an inhibitor. *Proc. Natl. Acad.*  
766 *Sci. USA.* 100 (2003) 13190-13195.
- 767  
768  
769  
770  
771  
772  
773  
774

Table 1. The novel unsymmetrical aromatic disulfide compounds and their SARS-CoV M<sup>pro</sup> inhibitory activities (*IC*<sub>50</sub>)

Entry no.	Chemical structure	<i>IC</i> <sub>50</sub> (μM)	Entry no.	Chemical structure	<i>IC</i> <sub>50</sub> (μM)
3-1		1.871±0.071	3-21		1.250±0.023
3-2		2.803±0.052	3-22		2.211±0.152
3-3		3.675±0.193	3-23		3.321±0.068
3-4		3.130±0.052	3-24		2.555±0.270
3-5		1.506±0.184	3-25		2.452±0.126

3-6		$4.344 \pm 0.538$	3-26		$1.679 \pm 0.042$
3-7		$4.100 \pm 0.832$	3-27		$1.557 \pm 0.116$
3-8		$1.762 \pm 0.044$	3-28		$1.713 \pm 0.052$
3-9		$5.654 \pm 0.259$	3-29		$1.118 \pm 0.132$
3-10		$4.511 \pm 0.105$	3-30		$1.264 \pm 0.033$

3-11		$5.794 \pm 0.050$	3-31		$0.516 \pm 0.060$
3-12		$2.626 \pm 0.082$	3-32		$0.921 \pm 0.060$
3-13		$1.651 \pm 0.048$	3-33		$1.437 \pm 0.053$
3-14		$2.075 \pm 0.016$	3-34		$1.121 \pm 0.060$
3-15		$5.954 \pm 0.363$	3-35		$1.991 \pm 0.086$
3-16		$3.957 \pm 0.190$	3-36		$1.495 \pm 0.055$

3-17		$4.126 \pm 0.094$	3-37		$0.883 \pm 0.028$
3-18		$2.565 \pm 0.075$	3-38		$0.684 \pm 0.012$
3-19		$1.947 \pm 0.508$	3-39		$0.697 \pm 0.053$
3-20		$2.029 \pm 0.488$	3-40		$1.522 \pm 0.214$

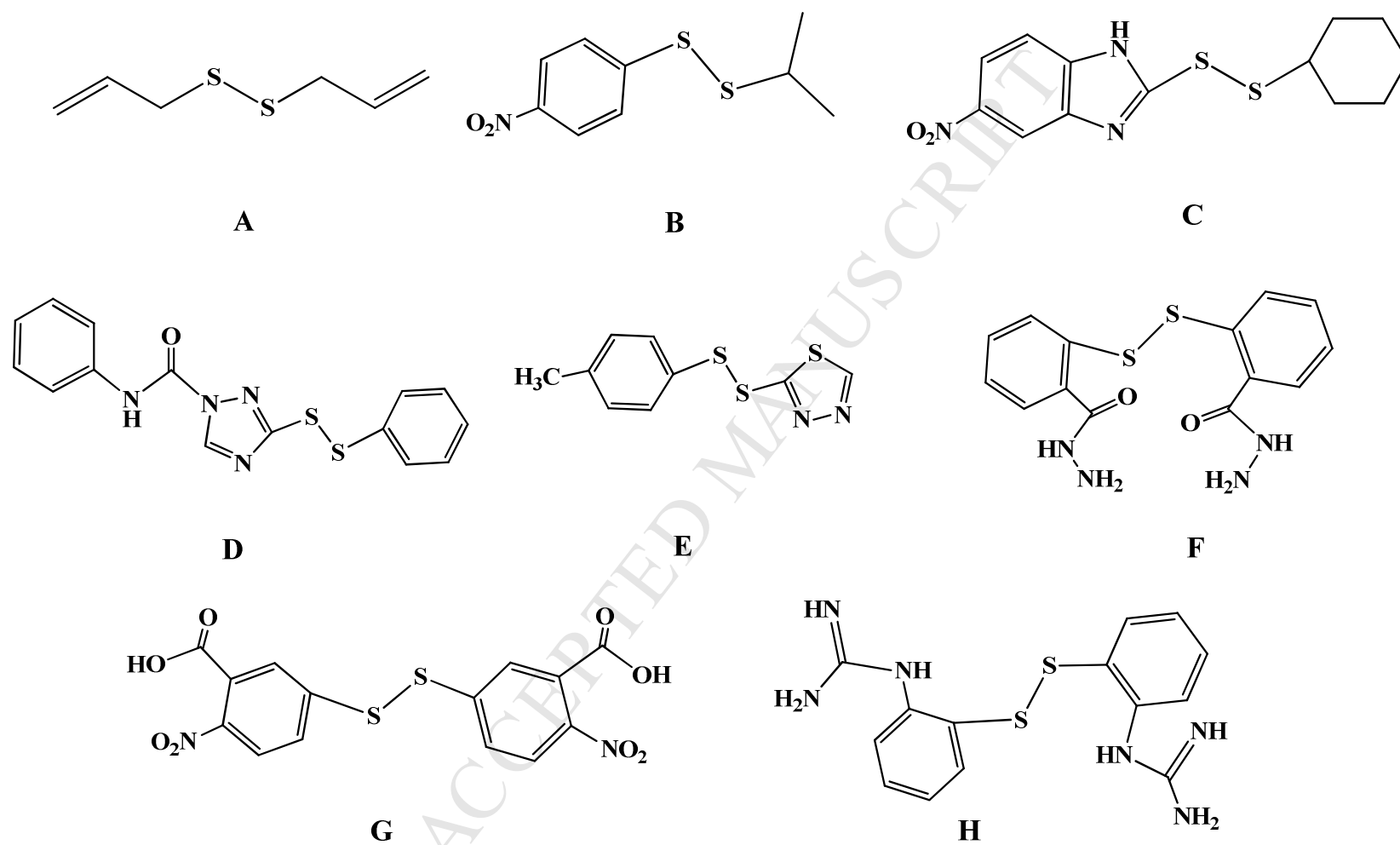
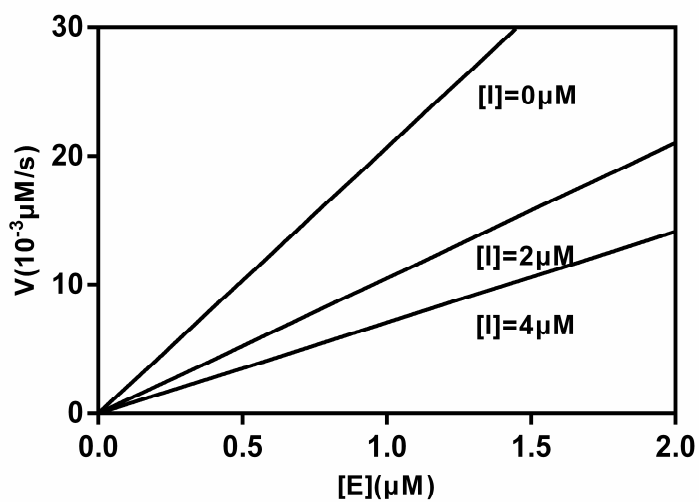
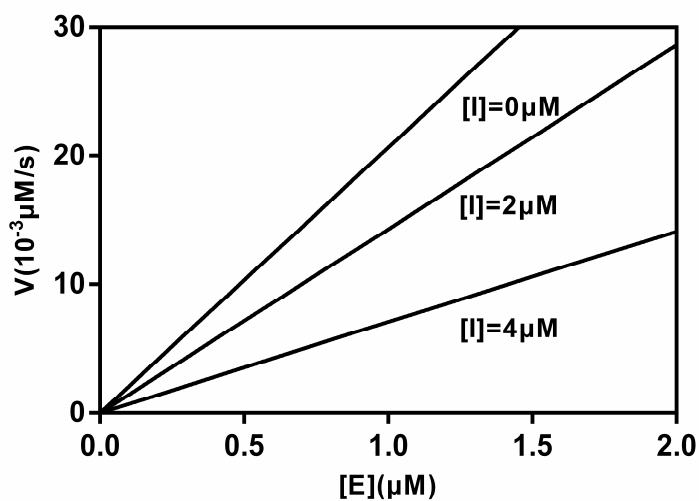


Fig. 1. Different disulfide compounds with various biological activities from literature.

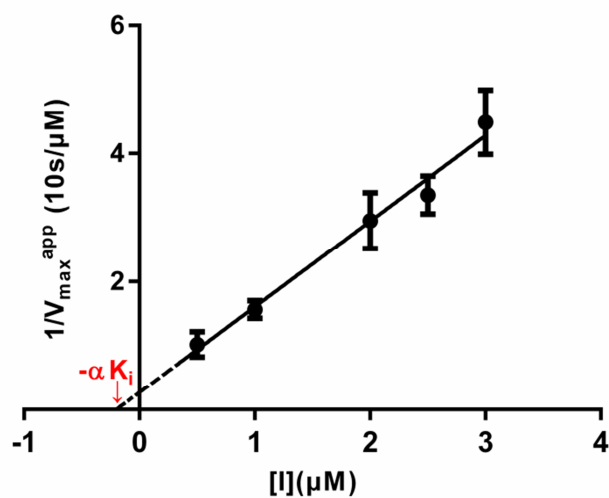


A

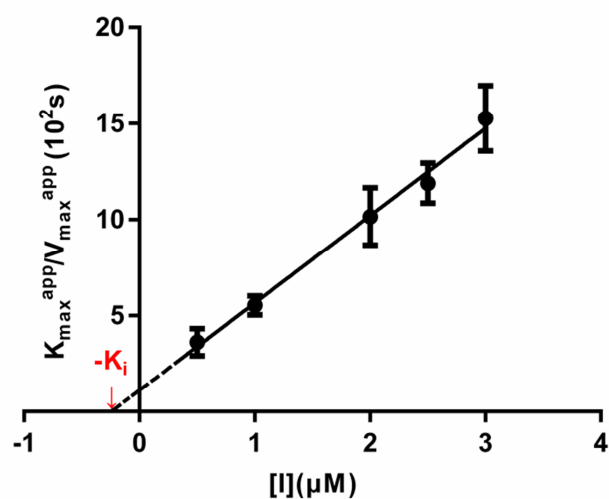


B

Fig. 2. Plot of enzyme concentration *versus* reaction velocity for enzymatic kinetic study of 3-31 (A) and 3-39 (B).



A



B

Fig. 3. Secondary plots for the determination of the kinetic constants ( $K_i$  and  $\alpha K_i$ ) of inhibitor 3-31 as a non-competitive inhibitor. The values of  $\alpha K_i$  (A) and  $K_i$  (B) are calculated from the  $x$  intercept.

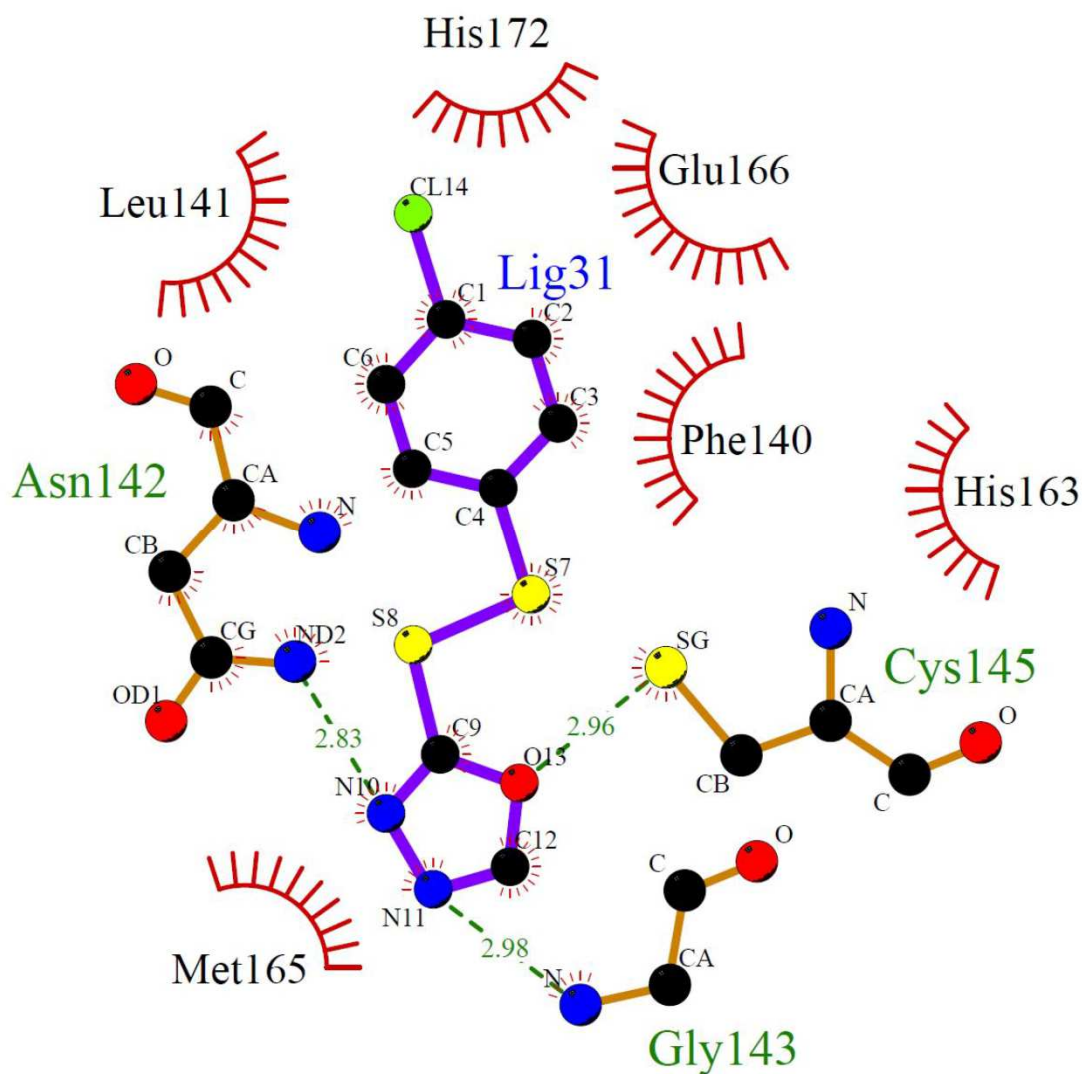


**Fig. 4. LIGPLOT 2D representation of 3-31 bound with SARS CoV Mpro from FlexX docking. The hydrogen bonds between the enzyme and the inhibitor are shown as green dashed lines, and distances are in Å units. Amino acid residues that are within van der Waals contact of the inhibitor are shown as red arcs.**

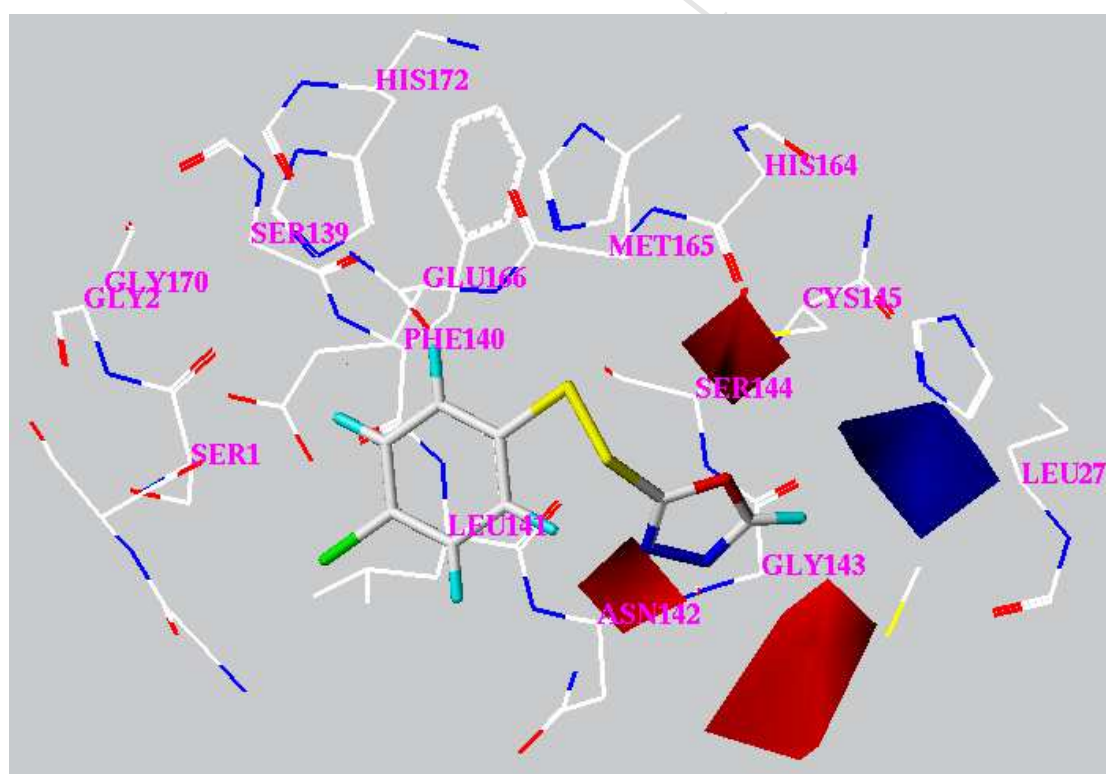
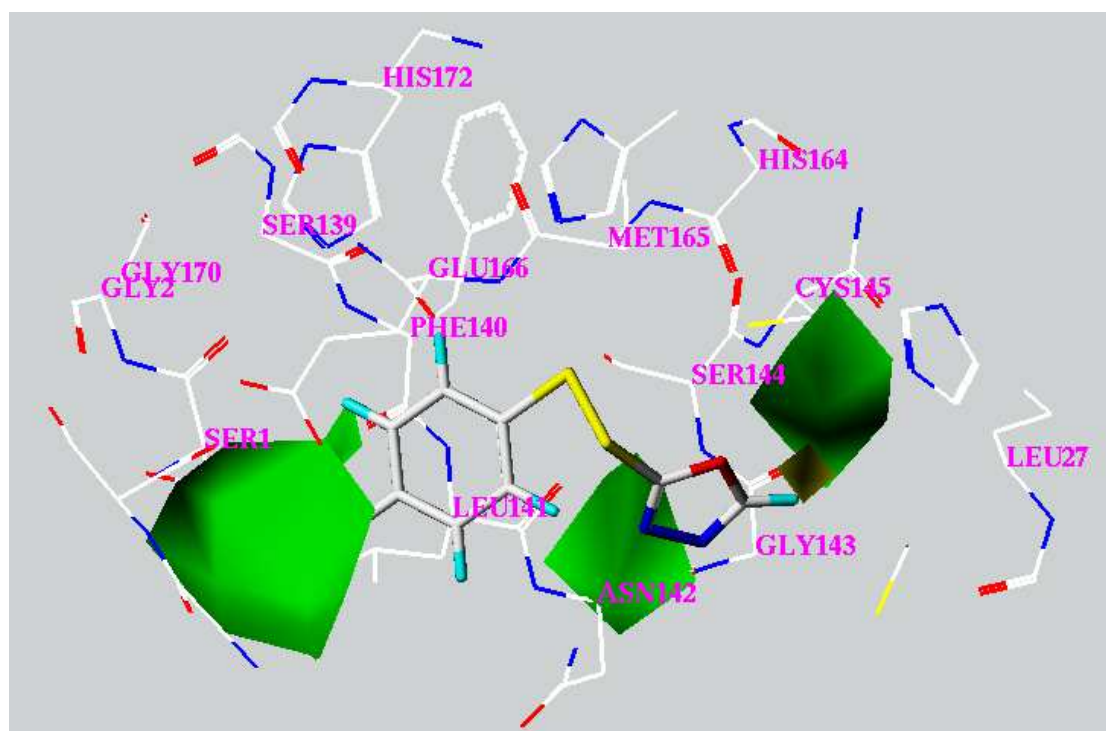
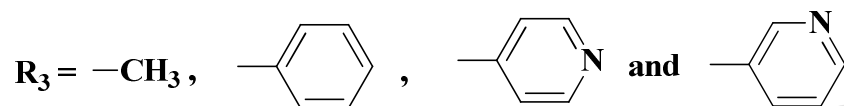
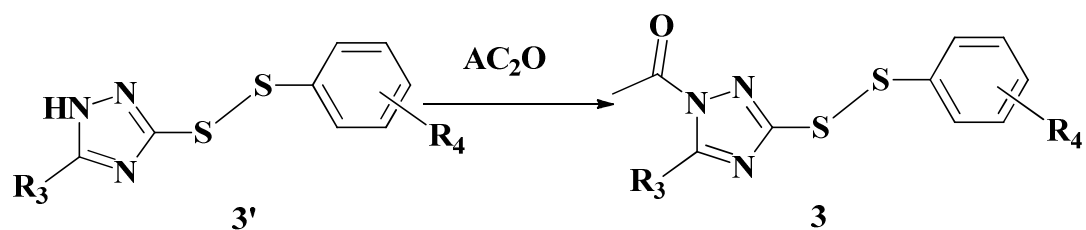


Fig. 5. Steric contour map (A) and electrostatic contour map (B) for the CoMFA model. Sterically favored and disfavored regions are shown in green and yellow in map A. Electrostatic favored and disfavored regions are shown in blue and red in map B.





**Scheme 2.** Synthesis route of the target unsymmetrical aromatic disulfide compounds (3-4, 3-6, 3-7, 3-8, 3-9, 3-10 and 3-11)

- 40 novel unsymmetrical aromatic disulfides were synthesized.
- The synthesized disulfide compounds are potent inhibitors of SARS main protease.
- Possible binding mode and structure-activity relationships of the compounds were established.

ACCEPTED MANUSCRIPT